Thermally Activated Delayed Fluorophore and Plasmonic Structures Integrated with Halide Perovskites for Efficient X-ray Scintillation and Imaging

Atanu Jana,[1] Sangeun Cho,[1] Kandasamy Sasikumar,[2] Heonkgyu Ju,[2,*] Hyunsik Im,[1,*] Robert A. Taylor[3]

[1]Division of System Semiconductor, College of AI Convergence, Dongguk University, Seoul 04620, Republic of Korea

[2]Department of Physics, Gachon University, Seongnam-si, 13120, Republic of Korea

[3]Clarendon Laboratory, Department of Physics, University of Oxford, Parks Road, Oxford OX1 3PU, UK

* Correspondence: batu@gachon.ac.kr (H.J.), hyunsik7@dongguk.edu (H. I)

ABSTRACT

The development of inexpensive and easily processable X-ray-sensitive materials is of great importance because a number of commercial scintillators, such as $LaBr_3$(Ce), $Gd_3Al_3Ga_2O_{12}$(Ce), Cs_2HfCl_6, NaI:Tl, CsI:Tl, and LiI:Eu, are fabricated using highly toxic or rare-earth elements via high-temperature synthesis. This has spurred research into radioluminescence-enhancing mechanisms and solution-processable scintillating materials made from earth-abundant elements that have excellent optoelectronic properties, including high-quantum yields and a low afterglow effect. In recent years, a range of metal halide perovskite (MHP) integrated with thermally activated delayed fluorescence (TADF) materials have been developed, exhibiting excellent scintillation properties and a high spatial resolution. Meanwhile plasmonic technologies are reported to exploit light energy confinement capabilities beyond the diffraction limit that produces local field enhancement. This enhancement has subsequently improved the performance of small-sized optoelectronic

devices such as solar cells and diagnostic optical sensors. This perspective summarizes the current development of MHP, TADF, and plasmonic materials for use in scintillators and their integrated moieties, while also identifying the relevant challenges. Following a thorough evaluation of the efforts made to improve the X-ray scintillation efficiency of these materials, we propose an outlook for future research in order to further enhance their scintillation properties and spatial resolution.

1. INTRODUCTION

Metal halide perovskites (MHPs) have gained significant research attention for their potential use in radiation detection due to their high X-ray absorption coefficients, high light yield, fast decay of X-ray-excited luminescence (XL), high charge carrier mobility, low afterglow, and tunable optical properties.[1–7] MHPs can also be fabricated using low-temperature solution processes, such as spin-coating and inkjet printing, which are cost-effective and scalable[8,9] meaning that they are compatible with existing α-Si readout electronics and are thus an attractive option for radiation detection in various applications, including medical imaging, security screening, and environmental monitoring. Conventional scintillators such as CsI:Tl, $Bi_4Ge_3O_{12}$, $PbWO_4$, and $YAlO_3$:Ce have been widely used for X-ray imaging, but their production requires expensive and time-consuming methods, such as Czochralski growth technique.[10,11] While MHP-based scintillators have exhibited outstanding performance, their hygroscopicity and elemental toxicity (such as lead(Pb)) have limited their practical application to date.[12] MHPs often suffer from unwanted internal losses due to surface defect-mediated absorption or scattering.

Thermally Activated Delayed Fluorescence (TADF) chromophores present several advantages as X-ray scintillators.[13] Their high photoluminescence quantum yield (PLQY)

indicates effective conversion of absorbed X-ray energy into emitted light. The high PLQY arises from their unique molecular structure whereby the reverse intersystem crossing (RISC) enables triplet excitons to transfer back to singlet ones, resulting in energies of both types of excitons being harvested into light emission.[14,15] These properties lead TADF to be highly sensitive X-ray scintillators. TADF materials often offer tunable emission wavelengths, providing flexibility in tailoring scintillator properties for specific applications. Additionally, their low toxicity is advantageous, particularly in medical applications. TADF materials have a relatively long excited-state lifetime (of the order of microseconds) due to the inherent quantum nature of the forbidden triplet-to-singlet transition. This long lifetime increases the probability of exciton quenching via inter-molecular interaction between triplet states or between triplet and singlet states, leading to a lower luminescence efficiency and a shorter operating lifetime. Therefore, reducing the excited-state lifetime is currently an important focus of research for the optimization of TADF materials.[16]

Some TADF materials are solution-processable, enabling the facile fabrication of thin films and coatings, while their molecular design flexibility allows for customization to optimize responses to specific X-ray energies. X-rays can be categorized as either "soft," characterized by energies typically below 10 keV, or "hard," with energies ranging from 10 to 200 keV.[17] The combination of efficient X-ray absorbers such as MHPs and luminescent centers such as organic TADF chromophores offers an advanced approach to the fabrication of high-performance organic-based X-ray imaging scintillators.[18] The design considerations for effective energy transfer in hybrid systems involving X-ray absorbers and TADFs encompass several key aspects. Firstly, the X-ray absorber should contain elements with a high atomic number (Z) to ensure a large X-ray absorption cross-section.[19] This is because the X-ray absorption cross-section is proportional to Z^a; where a is approximately 4 or 5 for certain X-ray energies.[20] This power-law dependence highlights the increased absorption efficiency

associated with higher atomic numbers. Therefore, materials with high-Z elements such as gold (Au), platinum (Pt), or bismuth (Bi) are often used as X-ray absorbers. Additionally, it's crucial to consider the X-ray energy in relation to the absorption edges of the material, as absorption characteristics can vary significantly depending on this factor. If the energy of the X-ray photon (typically below a few hundreds of keV) is below the absorption edge of a particular element, it is less likely to cause the photoelectric effect for that element.[18,21] In other words, the photon does not have enough energy to overcome the binding energy of the inner-shell electrons. Compton scattering takes place at relatively higher energies between a few hundreds of keV and ~ 1 MeV, whereas electron-positron pair creation becomes dominant at higher energies with an onset at ~1 MeV in interactions between X-rays and matter. Understanding these fundamental photon-matter interactions is essential for accurate predictions and optimizations in X-ray scintillation processes. When high-energy electrons interact with a material, they can indeed generate secondary electron-hole pairs through processes like electron-electron scattering. These secondary pairs can, in turn, contribute to additional ionization events. Furthermore, deep holes created in the initial ionization process may undergo Auger decay. Auger decay involves the transition of an outer-shell electron into a core hole left by the ejected inner-shell electron. During this process, energy is released and transferred to another bound electron, which is then ejected as an Auger electron. The Auger process can continue in a cascade fashion, with subsequent Auger electrons potentially leading to further ionization events and the release of additional electrons. This process increases the number of electron–hole pairs that are transferred to the luminescent center, which subsequently emits visible photons that are then detected by light detectors. Secondly, a robust interaction between the two components is essential to maintain a short distance between them. This proximity facilitates a swift and effective energy transfer mechanism. Thirdly, there must be a significant spectral overlap between the X-ray absorber and the TADF. This spectral alignment is crucial

as it serves as a fundamental prerequisite for ensuring a rapid and efficient energy transfer. Finally, it is advantageous to utilize TADFs that can simultaneously harness the energy from both singlet and triplet excited states. This approach is particularly effective since 25% of the excited states generated from ion recombination are singlet states, while the remaining 75% are in the form of triplet states. By leveraging both singlet and triplet excited states concurrently, the system can capitalize on a broader range of energy states, enhancing overall energy transfer efficiency.

The use of scintillators with large refractive indices such as MHPs tends to lead to poor light-detection efficiency because of index-contrast-induced light trapping within the material. However, this can be resolved by employing plasmonic technologies to create another non-radiative decay channel for the transfer of excitonic energy to surface plasmons. The decay processes strengthened by plasmonic local field enhancement eventually produces far-field radiation, consequently improving both light quantum yields and extraction efficiency.[22]

In this perspective, we examine the progress in the design and integration of innovative materials such as TADF, plasmonic structures, and MHPs (**Scheme 1**) for use in X-ray scintillators. We describe the X-ray scintillation mechanisms of these integrated materials and explore potential modifications to enhance their effectiveness. In particular, various strategies for enhancing the light yield using both individual and integrated structures are evaluated. Finally, drawing from recent advancements in scintillator materials, we propose a suitable configuration for an integrated device capable of high-quality X-ray imaging.

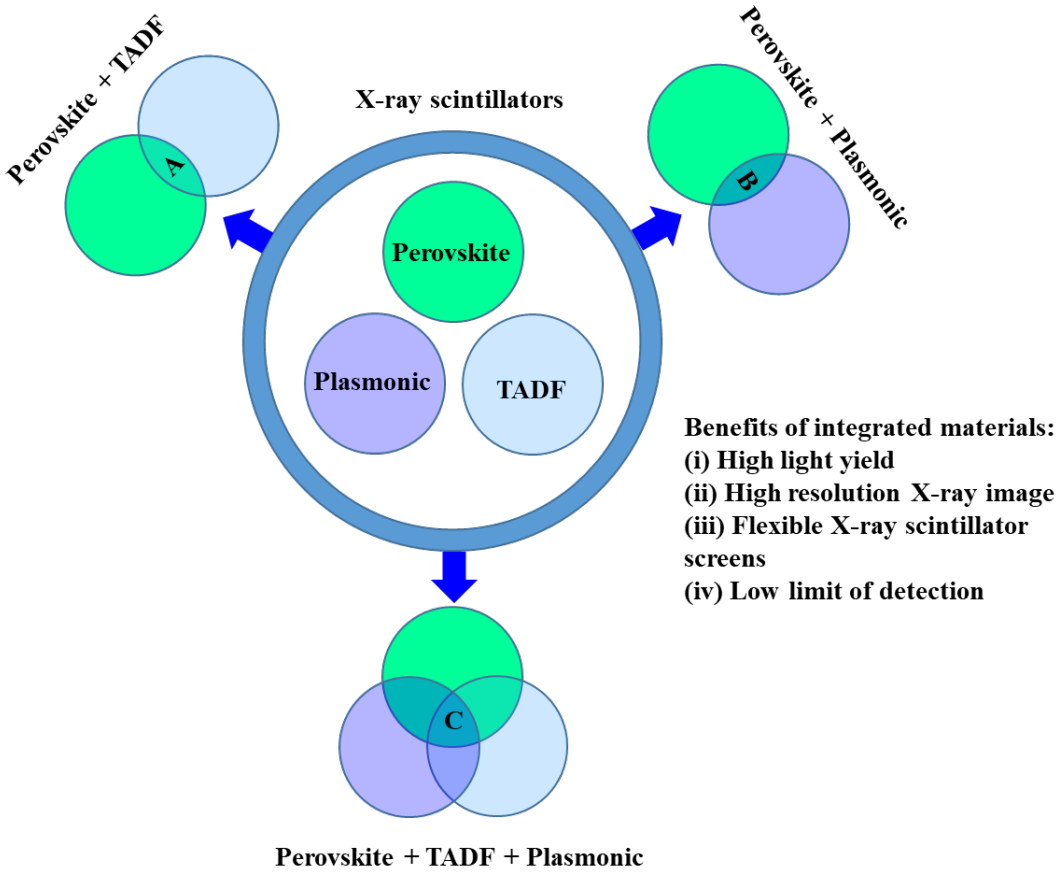

Scheme 1. Schematic diagram of different integrated X-ray scintillators. (A) MHPs and TADF (B) MHPs and plasmonic (C) MHPs, plasmonic, and TADF.

2. Scintillation mechanisms

Scintillation is a fundamental process observed in high-energy radiation-sensitive materials following exposure to ionizing radiation.[23] When radiation interacts with these materials, it excites electrons within their atomic or molecular structures, generating an excited state. Subsequently, when the excited electrons return to their ground state, they release excess energy in the form of photons, leading to the emission of light. The efficiency and characteristics of scintillation vary depending on the specific material involved,[24–29] in particular its atomic/molecular composition and spatial arrangement and the energy levels

involved in the excitation and de-excitation processes. Consequently, different materials vary in their scintillation characteristics, including their light yield, decay time, energy resolution, and sensitivity to various forms of ionizing radiation.

2.1 Thermally activated delayed fluorophores integrated with metal halide perovskites

The X-ray scintillation mechanism involving the integration of halide perovskites with thermally activated delayed fluorophores (TADF) is a multifaceted process that holds significant promise for revolutionizing X-ray detection and imaging technologies. At its core, this mechanism leverages the unique properties of halide perovskites and TADF materials to enhance the efficiency and sensitivity of X-ray scintillation. The scintillation mechanisms for MHPs can be generally grouped into three stages: conversion, transport, and radioluminescence (RL) (**Scheme 2**).[24] In the conversion stage, the incoming X-ray radiation interacts with the atoms of the scintillator **(Scheme 2A)**.[21] Various mechanisms, such as photoelectric absorption and Compton scattering are involved at this stage. The photoelectric effect and Compton scattering are the dominant mechanisms for the interaction between X-rays and matter at energies below 1 MeV. In the photoelectric effect, the atomic absorption of an X-ray photon causes an inner-shell electron to be ejected from the atom, leaving behind a vacancy (referred to as a hole). This ejected electron, known as an energetic photoelectron, can create additional electron–hole pairs through subsequent scattering with electrons of the material, with a larger probability with the electrons in the valence band. These secondarily generated hot carriers also undergo collisions to excite additional atoms, eventually leading to an electron cascade.

In Compton scattering, an X-ray photon collides with an outer-shell electron in an atom, causing the electron to recoil and the photon to scatter at a lower energy. These excited species can then undergo additional interactions, leading to the production of many secondary electrons and holes, which can further induce the production of electrons and holes through subsequent

collisions. As a result of this cascading collision process, the charge carriers eventually end up with a lower kinetic energy. The still-hot carriers then collide with phonons of the material lattice, resulting in carrier cooling for thermalization, in which a quasi-equilibrium forms with low-kinetic-energy electrons and holes in the conduction and valence bands, respectively. The entire process from absorption to carrier cooling typically takes place on a picosecond timescale before radiative recombination.[21]

In the transport stage of the scintillation process, the photo-generated and scattering-induced carriers from the conversion stage move through the scintillator material toward luminescence centers. The transport toward the luminescent center is due to mobility of charge carriers which recombine and emit visible photons. However, during this stage, the carriers can be captured by defects in the scintillator, such as ionic vacancies, grain boundaries, or impurities, which can lead to non-radiative losses and reduce the overall efficiency of the scintillator. Therefore, optimizing the crystal quality and surface morphology of the scintillation material to increase the yield from radiative recombination is important. The transport stage typically occurs within a time scale of 10^{-12} to 10^{-8} s.

To improve the conversion, transport, and radioluminescence (RL) of MHPs, a comprehensive range of approaches is necessary. The primary focus should be material engineering, i.e., optimizing the halide composition and cation mix to tailor the bandgap for efficient high-energy X-ray light absorption and conversion. In scintillation materials, optimizing the halide composition and cation mix to tailor the bandgap is critical for efficient light absorption and subsequent conversion processes. When exposed to X-rays, these materials absorb the incoming energy, promoting electrons to higher energy levels within the band structure. By precisely adjusting the halide composition and cation mix to modify the bandgap, one can ensure that the absorbed energy is sufficient to elevate electrons to the

conduction band. The subsequent recombination of excited electrons with holes in the valence band results in the emission of photons. Fine-tuning the bandgap through strategic halide and cation adjustments is paramount for optimizing this conversion process, as it directly influences the efficiency with which absorbed energy is translated into detectable light signals, thereby enhancing the overall performance of scintillation materials in radiation detection applications. Quantum confinement in nanostructured perovskites can also enhance these processes. Addressing defects through passivation techniques and co-doping with activator ions can subsequently improve carrier transport and radiative recombination efficiency. Advanced characterization methods, coupled with theoretical modeling, can also strengthen the understanding of RL mechanisms, making targeted improvements possible, while the control of structural features and the device architecture, such as grain boundaries and light extraction techniques, can enhance overall scintillator performance. Ultimately, the development of MHP materials with excellent thermal stability, reduced toxicity, and minimal environmental impact is required to ensure their practical applicability.

The final stage of the scintillation process is the release of scintillation photons. In case of MHP-TADF materials, another energy transfer process occurs between MHP and TADF materials (**Scheme 2B)**.[18] This promotes the efficient utilization of excitation energy, reduces energy loss due to non-radiative decay, and ultimately enhances the light yield, which is crucial for improving the performance and sensitivity of scintillation detectors. The energy transfer occurs from singlet excited state of MHP to singlet excited state of TADF. A singlet excited state can either decay radiatively to its ground state with the emission of a photon or decay non-radiatively to a triplet excited state (intersystem crossing). A triplet state cannot radiatively decay to the ground state due to quantum mechanical selection rules. However, in TADF materials, electrons can transfer from a triplet to a single state via thermal energy. This can be followed by transformation back to a triplet, eventually leading to continuous switching

between the two states, during which radiative decay from the single to the ground state can occur with photon emission. TADF materials often have complex molecular structures with electron-donating and electron-accepting moieties that facilitate efficient energy transfer between the singlet and triplet excited states. The efficiency of this process is quantified by the TADF rate constant, which is influenced by various factors such as the energy gap between the singlet and triplet states (also referred to as the singlet–triplet offset, ΔE_{ST}), the strength of the electron-donating and accepting groups, and the degree of molecular conjugation. TADF materials are particularly promising due to their small ΔE_{ST}, which allows for the efficient harvesting of luminescent species with carrier-populated excited states.

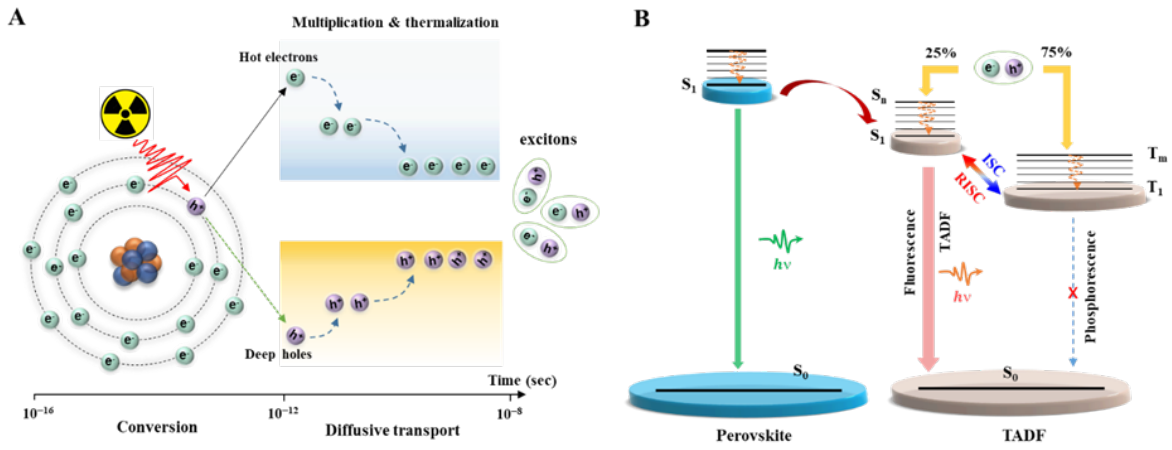

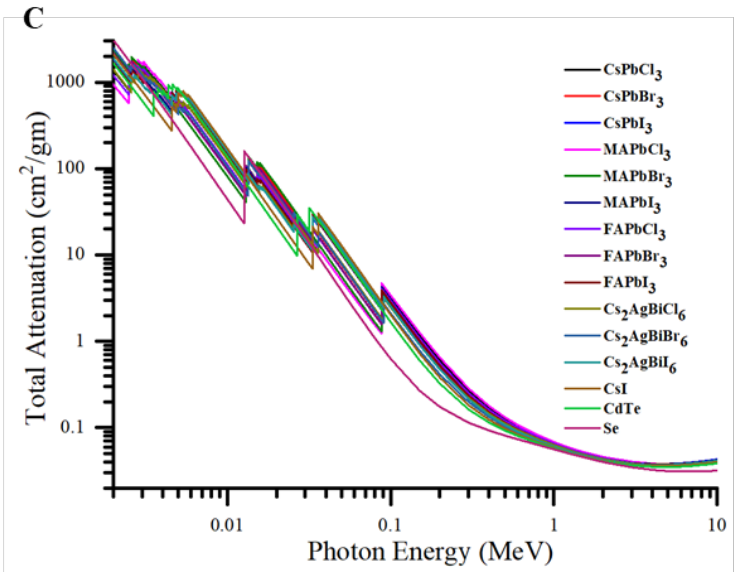

Scheme 2. (A) Scintillation mechanisms on an atomic scale (conversion and diffusive transport), (B) enhanced radioluminescence via energy transfer from the MHP to TADF in hybrid MHP-TADF materials, and (C) attenuation coefficients of selected perovskites and well-known commercial X-ray-sensitive materials as a function of the photon energy. Attenuation data are taken from the NIST-XCOM database.[30]

In semiconductors such as MHPs and CdTe, which contain elements with a high atomic number such as lead (Pb), bismuth (Bi), iodine (I), and cadmium (Cd), the higher number of electrons per atom enhances these interactions compared to elements with a low atomic number, such as Se (atomic number = 34).[31] Consequently, as shown in **Scheme 2C**, these materials exhibit higher attenuation coefficients[30] when exposed to photons with energies ranging from tens to hundreds of kiloelectronvolts (keV). An X-ray absorber with a high atomic number can be conjugated with a TADF material. When the X-ray-absorbing species (e.g., a halide perovskite) absorbs X-rays, it is excited to a higher energy state. Through Förster resonance energy transfer (FRET), the energy from this excited X-ray absorbing species is transferred to the luminescent center of the TADF material,[18] leading to a higher efficiency in converting X-ray energy to visible light energy because excitation occurs through both triplet and singlet states. This produces a high PLQY and a long emission lifetime, meaning that TADF materials have significant potential as highly efficient next-generation scintillators for use in various applications.

2.2 Plasmonic structures integrated with metal halide perovskites

Surface plasmons (SPs) arise from the coherent interaction between light and the collective oscillation of free electrons at the metal-dielectric-interface. While a flat metallic surface supports the propagating mode of SPs (i.e., polaritons), a three-dimensional metallic nanostructure can produce a non-propagating mode, (i.e., localized SP resonance LSPR). Noble

metallic nanostructures allow LSPR to be excited at visible or near-infrared wavelengths. Plasmonic nanostructures provide the means of confining light energy within the subwavelength region, leading to locally enhanced fields. The use of plasmonic technologies to enhance X-ray scintillation efficiency has been demonstrated recently.[22]

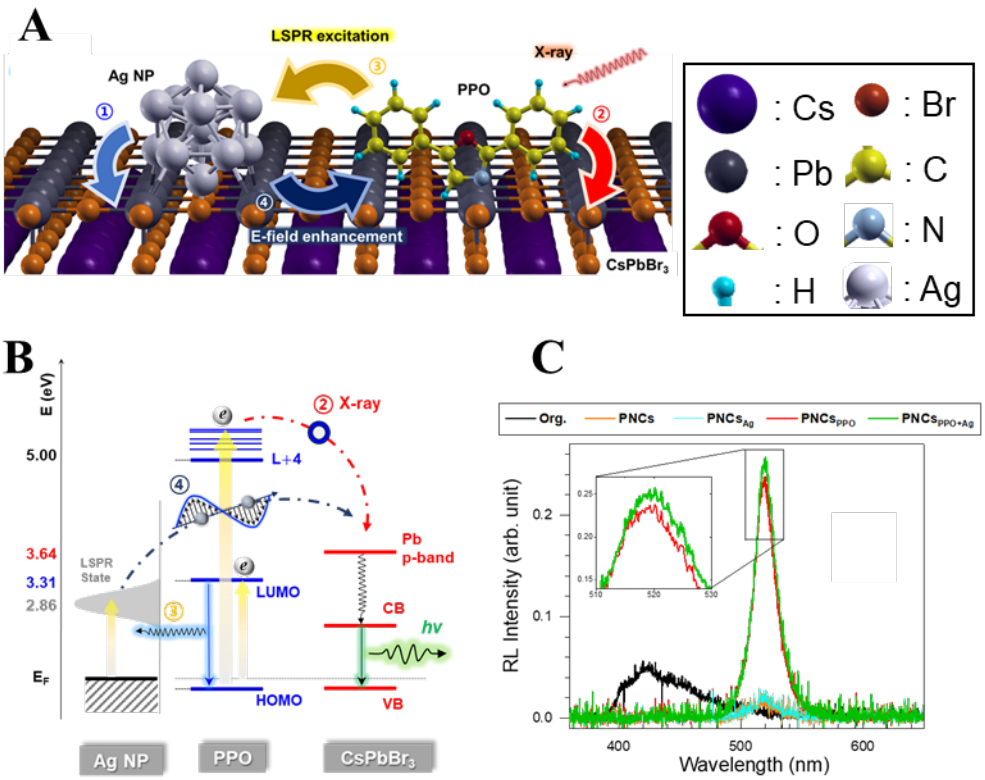

Scheme 3. (A) Schematic of hybridized scintillators consisting of PPO, AgNPs, and $CsPbBr_3$ for X-ray scintillation. (B) Mechanisms underlying enhanced X-ray scintillation based on the energy levels. (C) Enhanced RL of hybrid scintillators under X-ray illumination. Reproduced with permission.[22] Copyright 2023, Wiley-VCH GmbH, Weinheim

As shown in **Scheme 3A-C**, organic molecules of 2,5-diphenyloxazole (PPO), Ag nanoparticles (NPs), and colloidal perovskite nanocrystals of $CsPbBr_3$ were combined to create a hybrid scintillator that exhibited enhanced RL under X-ray illumination.[22] Photo-generated carriers, (i.e., electrons and holes) in PPO under X-ray illumination were then transferred to the luminescent centers of $CsPbBr_3$ via FRET. In addition, spectral overlap between the excited

PPO molecules (with an excited state energy band of 400–450 nm) and the LSPR of Ag NPs centered at 433 nm lead to plasmonic excitation. The subsequent coupling between the plasmons and luminescent centers of $CsPbBr_3$ facilitated the efficient charge transfer from PPO excited states to the luminescent centers. Given the ease of fabrication for this hybrid material, the Ag NP-mediated enhancement of $CsPbBr_3$ emissions may inspire the development of future hybrid materials for X-ray scintillation in medical and industrial applications.

If a TADF molecule is used instead of 2,5-diphenyloxazole (PPO) in the hybrid scintillator, the dynamics of the charge transfer and excitation mechanisms are likely to undergo significant changes. TADF molecules can potentially enhance the transfer of photo-generated carriers from the organic matrix to the luminescent centers of $CsPbBr_3$ via FRET.[18] With an excited state energy band that differs from that of PPO, TADF molecules may alter the spectral overlap with the plasmonic resonance of Ag NPs, potentially affecting the plasmonic excitation efficiency.[22] However, the outcome also depends on the specific properties of the TADF molecules employed and their compatibility with the overall hybrid system.

2.3 Metallic plasmonic nanostructures for enhanced scintillator efficiency

Scintillators emit light in visible or UV region after being irradiated by sources with large photon energies, such as X-rays and gamma rays. They are used in either a solid or liquid phase and consist of photon emitters that are more complex than typical fluorophores in terms of their excitation mechanisms.[28] Scintillators have found numerous applications, such as in nuclear medical imaging,[29] high-energy physics experiments,[32] and border screening,[33] thus there is continuous demand for brighter, faster, and more cost-effective devices. However, most scintillators suffer from low extraction efficiency for luminescent energy due to their intrinsically high index of refraction, causing luminescence to be trapped by total internal reflection.[34] This results in an inherently low external quantum efficiency.

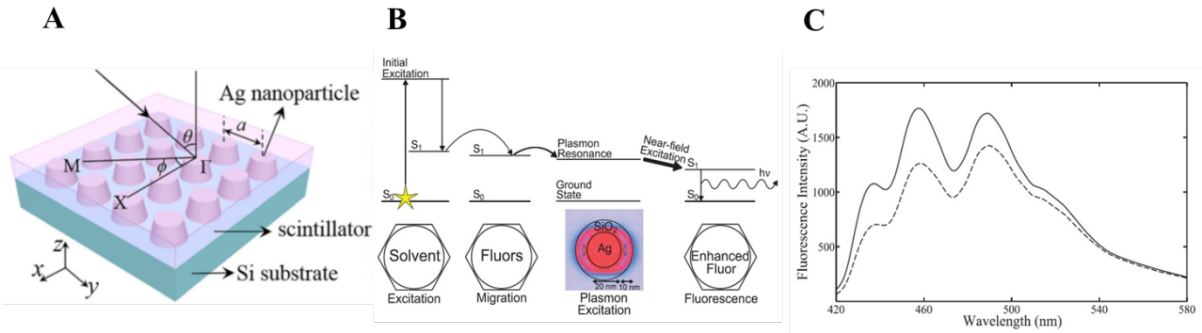

Figure 1. (A) Surface lattice resonance of an Ag nanoparticle array, Copyright 2021, AIP Publishing.[35] (B) FRET-induced excitation chain using localized SPs. (C) Plasmonic NP-induced enhancement of fluorescence. Reproduced with permission. Copyright 2021, AIP Publishing.[28]

It has been reported that the extraction efficiency can be enhanced using photonic crystal structures,[36–38] such as nanostructures consisting of protruding dielectrics with a high refractive index (e.g., moth-eye patterns).[34] It has also been found that SP technologies can enhance the extraction efficiency when used to generate surface lattice resonance via an array of metal nano-antennas,[35,39] as shown in **Figure 1**. Individual localized SPs couple with each other via radiative coupling, resulting in diffraction-like effects, i.e., the directional radiation of luminescence[35,39]. These effects enhance the luminescence extraction efficiency. The surface resonance lattice allows the extended coupling with scintillator emitters that are even micrometers away while benefitting higher quality factors of its resonance than individual LSPR.

Ag-SiO_2 nanocomposites with a core–shell structure have also been reported to enhance the light yield of liquid-based scintillation using FRET in the excitation chain (**Figure 1B**).[28] The absorption and emission spectra of the relevant molecules need to substantially overlap for

FRET to occur. Fluorophores that are excited by solvent excitation transfer couple with composite NPs with emission wavelengths matching with the LSPR. The excited SPs are involved in near-field interactions with fluorophores, i.e., the 9-aminoacridine covalently bound to the surface of the NPs. This enhances the scintillator fluorescence (**Figure 1C**) due to the large optical absorption cross-section of the Ag NPs derived from local field enhancement around the NPs.

3. STRATEGIES FOR THE ENHANCEMENT OF THE LIGHT YIELD

3.1 Compositional and dimensional engineering

Compositional and dimensional engineering are important strategies for tailoring the scintillation properties of perovskite materials.[40,41] Because perovskite scintillators can emit light when exposed to ionizing radiation, they are valuable for various radiation detection and imaging applications. Compositional engineering involves modifying the chemical composition of the perovskite material to achieve the desired scintillation properties, which can be achieved by substituting different elements within the perovskite crystal structure or by introducing dopant ions.[42] The energy deposition, light yield, emission wavelength, and other scintillation parameters can be adjusted by carefully choosing the composition. For example, in lead halide perovskites, such as $CsPbBr_3$ or $CsPbI_3$, compositional variation can be employed to tune the bandgap and efficiently absorb ionizing radiation, while adjusting the halide composition can tailor the emission wavelength to match specific detector requirements.[43] Doping with appropriate ions can also enhance the scintillation efficiency, improve the charge transport properties, and reduce self-absorption.[44]

Dimensional engineering refers to the control of the size and morphology of perovskite crystals or nanostructures. The size of the perovskite grains, the presence of nanoscale features, or the use of thin films or nanostructured architectures can significantly impact the scintillation performance. For example, the use of nanosized crystals can improve the light yield, accelerate scintillation decay, and enhance the energy resolution due to the higher surface-to-volume ratio, which promotes efficient charge carrier transport and reduces non-radiative recombination. By tailoring their chemical composition and manipulating their structural characteristics, the performance of perovskite scintillators can be optimized for various radiation detection and imaging applications.[42]

Hybrid perovskites have an advantageous band gap in the visible region, leading to an improved light yield compared to traditional scintillators. However, despite a theoretical yield of 129,000–250,000 photons/MeV for hybrid perovskites, this has not yet been achieved. In particular, 3D hybrid perovskites typically produce a significantly lower light yield ~1,000 photons /MeV at ambient temperatures. Researchers have developed several strategies over the past few decades to address this disparity and enhance the light yield of hybrid perovskites for X-ray detection and imaging applications. These include manipulating the quantum confinement effect and self-absorption in hybrid perovskites, establishing energy-transfer channels, and modifying defects within the material.

The light yield of MHP scintillators is primarily influenced by the properties of excitons, particularly the exciton binding energy (E_b), which represents the energy required to separate excitons forming free electrons and holes. In bulk 3D hybrid perovskite scintillators, a low light yield of ~1,000 photons/MeV is associated with a low E_b (a few tens of meV). This indicates that the exciton states are loosely bound, and significant thermal dissociation occurs. In addition, as E_b increases, the population of excitons also increases. Therefore, improving E_b in

hybrid perovskites is an effective approach to increasing the light yield. It can be achieved by modulating quantum confinement via the reduction of the structural dimensions and crystal size, such as using QDs. In addition, introducing structural distortion in the crystal structure is also an effective strategy to increase E_b in hybrid perovskites, leading to improved light yields.

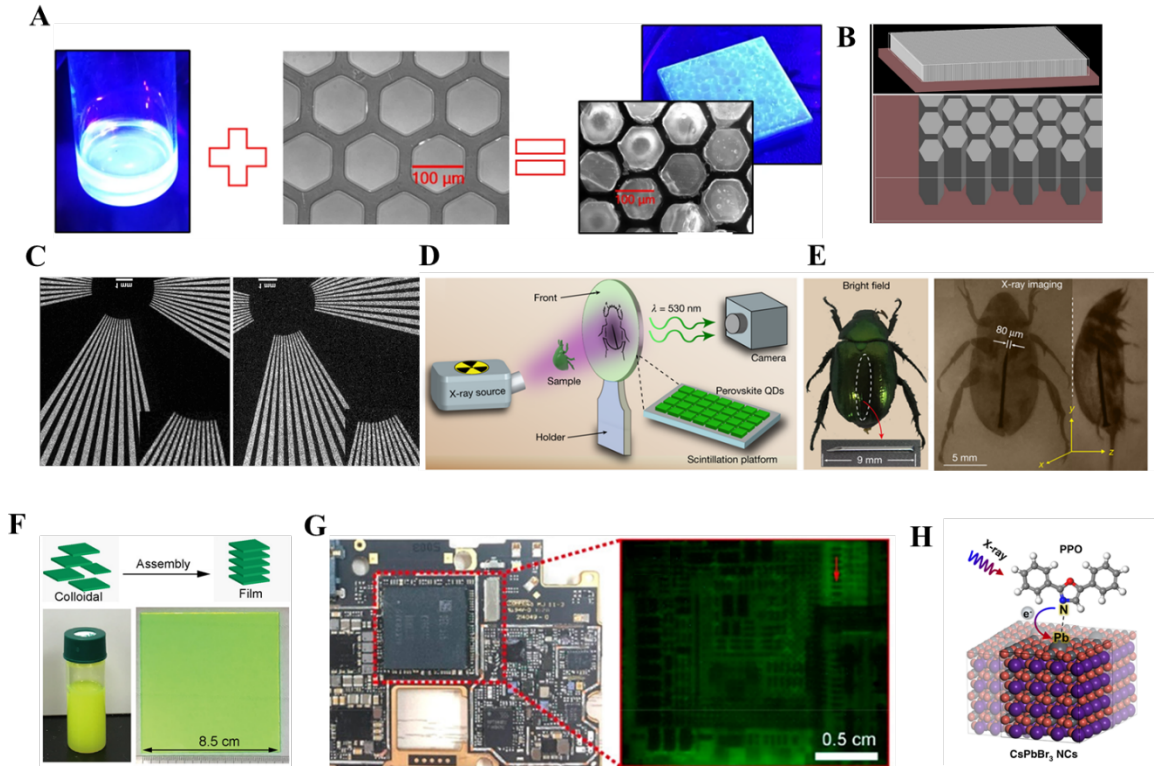

Figure 2. (A) X-ray imaging detector made of a microcapillary and Li-$(PEA)_2PbBr_4$ scintillator. (B) Borosilicate glass faceplate with 100-µm hexagonal capillaries that contain Li-$(PEA)_2PbBr_4$ in the Geant4 variant. (C) Images of the same resolution target taken using a Timepix camera with a Si sensor (left) and a Li-$(PEA)_2PbBr_4$ camera (right).[45] Copyright 2021 Nature Publishing Group. (D and E) Experimental setup and X-ray images of the biological samples.[46] Copyright 2018 Nature Publishing Group. (F) Diagram depicting the formation of $CsPbBr_3$ nanosheets through self-assembly (top). Images of dense colloidal $CsPbBr_3$ nanosheets in a toluene solution (left) and a wafer-sized thin layer on a glass slide (right). (G) Digital image of a transistor panel of a cell phone (left) and corresponding X-ray image

(right).[47] Copyright 2019 American Chemical Society (H) Schematic illustration of the $CsPbBr_3$ NC hybridized with PPO. Copyright 2020 Nature Publishing Group.[8]

In organic–inorganic hybrid perovskites, one useful way to reduce the structural dimensions is to enlarge the organic ligands, which leads to a change in the crystal structure, resulting in a two-dimensional (2D) perovskite structure.[48] It has been observed that the E_b of 2D halide perovskites is four times higher than that in 3D perovskites, which indicates that the excitons in 2D perovskites are more tightly bound. By increasing E_b through the reduction of structural dimensions, such as transitioning from 3D to 2D perovskite structures, the light yield of the hybrid perovskite scintillators can be improved. In 3D perovskites such as $MAPbBr_3$ and $MAPbI_3$, E_b has a range of 2–70 meV. However, for 2D perovskites, specifically (EDBE)$PbCl_4$ (EDBE=2,2'-(ethylenedioxy)bis(ethylammonium)), E_b is approximately 360 meV.[49] At 10 K, the light yield of 3D $MAPbBr_3$ and $MAPbI_3$ was 152,000 and 296,000 photons/MeV, respectively,[50] but these yields were dramatically reduced by thermal quenching to below 1000 photons/MeV at ambient temperatures. In contrast, 2D (EDBE)$PbCl_4$ was more resistant to thermal quenching, as evidenced by its light production of 9000 photons /MeV at ambient temperatures.

The transition from three-dimensional (3D) to two-dimensional (2D) perovskite structures in hybrid perovskite scintillators offers the advantage of improving the exciton binding energy (E_b) and subsequently enhancing the light yield. However, this process also faces several challenges. One of these is related to the engineering and synthesis of stable and reproducible 2D perovskite structures with large organic ligands. Achieving precise control over the crystal structure while maintaining stability and reproducibility on a large scale is a complex task. The synthesis of 2D perovskites requires careful optimization to prevent defects or variation in the crystal lattice that could affect the scintillation performance. Another challenge is balancing the trade-off between an enhanced E_b and an efficient light yield. While increasing E_b via the

transition to 2D perovskite structures can improve exciton binding, it may also impact other optical properties, such as the radiative recombination rate. Finding the optimal balance between these factors is crucial to achieving both a high Eb and efficient light emission. In addition, addressing challenges related to thermal stability is essential. While 2D perovskites exhibit improved resistance to thermal quenching compared to their 3D counterparts, maintaining high light yields at ambient temperatures remains a challenge. Developing strategies to enhance the stability of 2D perovskite scintillators under a range of temperatures and environmental conditions is crucial if they are to be employed in practical applications. In general, 2D-MHPs exhibit higher stability compared to their 3D counterparts. However, 3D-MHPs boast a higher PLQY than 2D MHPs. Given this trade-off, there is an urgent need to focus on the development of 2D-MHPs in order to enhance the scintillation yield and improve X-ray imaging, given that the inherent stability of 2D-MHPs can be advantageous in practical applications. Balancing stability with enhanced PLQY is crucial for optimizing the performance of materials used in scintillation and X-ray imaging technologies. The ongoing research and development efforts in this direction aim to harness the strengths of 2D-MHPs to address these specific challenges in the field.

The study by Dang et al. also demonstrated the potential of Li-doped $(PEA)_2PbBr_4$ as a scintillator for X-ray imaging.[51] The introduction of Li^+ as a dopant represents a valuable approach to enhancing scintillation properties by mitigating thermal quenching and improving light yields, ultimately benefiting X-ray imaging. By incorporating Li^+, the researchers observed an improvement in the light yield of $(PEA)_2PbBr_4$ from 8,000 to 11,000 photons/MeV. In a subsequent study by Motakef et al., a special X-ray imaging detector was fabricated using single Li-doped $(PEA)_2PbBr_4$ crystals synthesized. These crystals were synthesized inside the pores of a precast microcapillary plate, which had a thickness of 1.2 mm (**Figure 2A–C**).[45] This fabrication technique resulted in a thick film detector that exhibited a higher energy

absorption efficiency for X-rays. By incorporating microcapillaries within the detector, the isotropic propagation of emitted photons was constrained. This constraint led to the imaging detector achieving an impressive spatial resolution of 8.8 line pairs per millimeter (lp/mm) at a modulation transfer function (MTF) of 10%. Notably, this spatial resolution was on par with that of a direct Si detector, which typically attains 8.6 lp/mm at an MTF of 10%.

While the use of Li-doped $(PEA)_2PbBr_4$ as a scintillator for X-ray imaging shows promise, there are challenges associated with this process. One challenge involves the optimization of the Li+ doping concentration to achieve the desired enhancement of the scintillation properties. Finding the right balance is crucial because an excessive or inadequate amount of the Li+ dopant may impact the light yield and overall performance of the scintillator. Precise control over the doping process is necessary to ensure consistent and reproducible results in terms of an improved light yield and reduced thermal quenching. The fabrication of an X-ray imaging detector using Li-doped $(PEA)_2PbBr_4$ crystals within a precast microcapillary plate faces challenges related to scalability and manufacturability. Scaling up the production of such detectors while maintaining a uniform crystal quality and distribution within the microcapillary plate can be complex. Achieving reproducibility and consistency in the fabrication process is essential for practical applications.

Moreover, the incorporation of microcapillaries within the detector, while enhancing the energy absorption efficiency for X-rays, introduces challenges related to the design and engineering of the detector. The spatial arrangement and dimensions of the microcapillaries must be carefully controlled to optimize the isotropic propagation of emitted photons and achieve the desired spatial resolution. Fine-tuning these parameters to ensure optimal performance across various imaging conditions is a non-trivial task. In addition, while a spatial resolution of 8.8 line pairs per millimeter (lp/mm) is impressive, sustaining this resolution

under different imaging scenarios and over extended periods remains a challenge. Long-term stability, robustness under varying environmental conditions, and compatibility with diverse X-ray imaging applications require careful consideration and further research. Addressing these challenges is essential for realizing the full potential of Li-doped $(PEA)_2PbBr_4$ scintillators in advanced X-ray imaging systems.

In a similar manner to hybrid perovskites, 3D all-inorganic bulk HPs also encounter thermal quenching due to their low activation energy (E_b). For instance, at room temperature, $CsPbCl_3$ single crystals produce a light yield of around 300 photons/MeV, while $CsPbBr_3$ single crystals yield 50,000 photons/MeV at 7 K.[52,53] To address this challenge, researchers have looked to reduce the size of the perovskites, which effectively confines the excitons generated by X-ray irradiation within a limited space. By reducing the crystal size, the overlap of exciton wavefunctions within the nanocrystals increases. This confinement within a reduced Bohr radius consequently leads to an enhanced E_b.[54] The higher E_b resulting from the confinement of excitons in nanocrystals or QDs is a promising strategy for mitigating thermal quenching and improving the light yield of all-inorganic bulk hybrid perovskite materials. This approach offers potential benefits for X-ray detection and imaging applications by enhancing the efficiency and performance of hybrid perovskite scintillators. In 2017, Tang et al. conducted pioneering research demonstrating the scintillating properties of $CsPbBr_3$ QDs in various solvents upon X-ray irradiation.[55] This breakthrough study generated significant interest, and extensive research has subsequently focused on utilizing perovskite QDs as scintillators and X-ray imaging applications. In 2018, Liu et al. published a study introducing a series of $CsPbX_3$ NCs as scintillators with tunable emission wavelengths (**Figure 2D and E)**.[46] Tailored anionic components facilitates tunability. The thin-film scintillator based on $CsPbBr_3$ NCs exhibited remarkable performance attributes, including a low X-ray detection limit of 13 nGy/s and an impressive spatial resolution of 2.0 lp mm^{-1} at an MTF of 72%.

Notably, the spatial resolution achieved by this $CsPbBr_3$ NCs-based thin-film scintillator surpassed that of conventional $CsI:Tl^+$-based detectors, which typically achieve a spatial resolution of 2.0 lp/mm at a much lower MTF (36%). In X-ray imaging applications, large-area scintillator films play a vital role, but with perovskite QDs has been a challenging task. To overcome this hurdle, researchers often disperse perovskite QDs within various matrices, including organic polymers or glass. However, Mohammed and colleagues presented an innovative approach to tackle this issue. They employed a self-assembly process in a highly concentrated $CsPbBr_3$ solution, successfully demonstrating a novel technique for creating a large-area scintillator film of 72 cm^2 composed of $CsPbBr_3$ nanosheets (**Figure 2F and G**).[47] Exposure to X-rays revealed the film's exceptional long-term stability, accompanied by a remarkable light yield of 21,000 photons/MeV.

To further enhance the scintillation and X-ray imaging capabilities of perovskites, MHPs have been combined with organic molecules with matching energy levels. This approach promotes efficient charge transfer between the MHPs and organic fluorophores, thereby increasing the light yield of the combining species. Our group previously fabricated a hybrid liquid scintillator made of $CsPbBr_3$ QDs and 2,5-diphenyloxazole (PPO).[8,56] We matched the energy levels between PPO and $CsPbBr_3$ QDs using surface hybridization via N-Pb bonding (**Figure 2H)**, which facilitated charge transfer from PPO to $CsPbBr_3$ QDs upon X-ray irradiation. Consequently, the scintillation and X-ray imaging resolution were improved than pure PPO or $CsPbBr_3$ alone. This strategy of combining organic molecules with matching energy levels with hybrid perovskite scintillators holds promise for optimizing their sensitivity and the image quality in X-ray detection and imaging applications. The reverse engineering of the energy transfer process, in which energy moves from the perovskite to TADF organic molecules, holds significant promise for X-ray scintillation and imaging applications. For example, Mohammed et al. engineered a highly efficient X-ray harvesting system by

combining $CsPbBr_3$ nanosheets (D) with difluoroboron 1,3-diphenylamine β-diketonate (A).[18] $CsPbBr_3$ nanosheets were employed due to their high atomic number, high PLQY, broad absorption band in the green and blue spectral range, and strong emission band at 510 nm. In their system, A exhibits TADF properties, allowing for the efficient harnessing of both singlet and triplet excitons, with a broad absorption band from 400 to 600 nm that closely matches the emission spectrum of D **(Figure 3A)**. This spectral overlap facilitates an interspecies energy transfer of ~100%, with the optimized D-A composite film only exhibiting an RL emission peak at 620 nm. Additionally, the presence of two fluorine atoms in the A derivative enables strong bonding with the lead atoms within the perovskite nanosheets, enhancing the energy transfer efficiency **(Figure 3B)**. The fabricated X-ray imaging scintillator achieved a high imaging resolution of 135 μm and an impressively low detection limit of 38.7 $nGys^{-1}$.

Thermal quenching in X-ray scintillators represents a significant drawback, lowering their efficiency by reducing the scintillation output at higher temperatures. This limitation restricts their operating temperature range and reduces their sensitivity in X-ray detection applications. Thermal quenching also leads to lower imaging quality by reducing the resolution and contrast, thus affecting the reliability of X-ray imaging, while higher noise levels affect measurement precision. Similarly, long-term exposure to higher temperatures accelerates material degradation within the scintillator, shortening its lifespan and requiring frequent maintenance or replacement. To resolve these issues, multi-excited state switching has been proposed as a means to enhance the luminescence efficiency even at elevated temperatures. As an example of this, Wang et al. synthesized a zero-dimensional hybrid perovskite based on $TpyBiCl_5$, utilizing terpyridine (Tpy) and bismuth halide ($BiCl_3$) as its organic and inorganic constituents, respectively **(Figure 3C)**.[57] The $TpyBiCl_5$ crystal RL spectrum reveals two distinct emission bands: one at 494 nm, attributed to prompt fluorescence and TADF, and another at 568 nm, stemming from phosphorescence. Notably, the RL intensity correlates linearly with X-ray dose

A

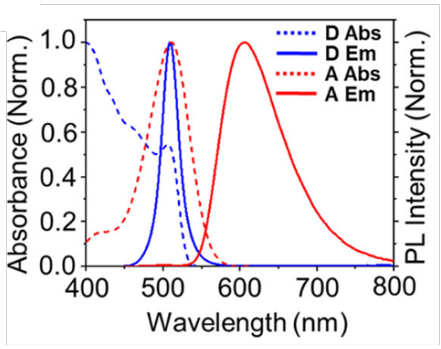
D Abs
D Em
A Abs
A Em
Absorbance (Norm.)
PL Intensity (Norm.)
Wavelength (nm)

B

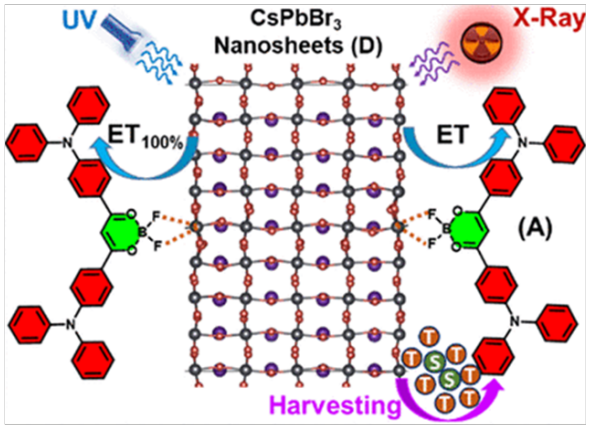
UV
CsPbBr3
Nanosheets (D)
X-Ray
ET100%
ET
(A)
Harvesting

C

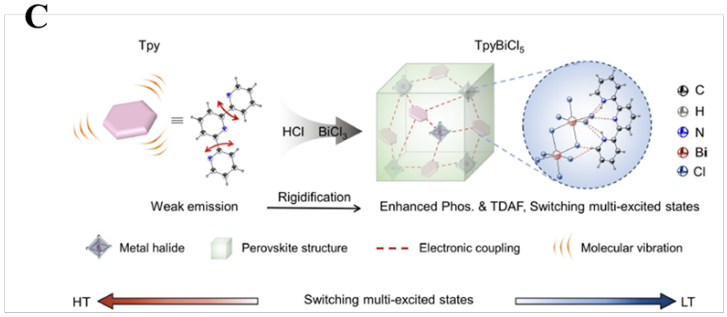
Tpy
TpyBiCl5
HCl
BiCl3
C
H
N
Bi
Cl
Weak emission
Rigidification
Enhanced Phos. & TDAF, Switching multi-excited states
Metal halide
Perovskite structure
Electronic coupling
Molecular vibration
HT
Switching multi-excited states
LT

D

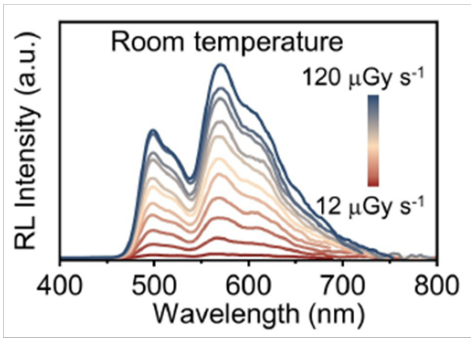
Room temperature
120 μGy s-1
12 μGy s-1
RL Intensity (a.u.)
Wavelength (nm)

E

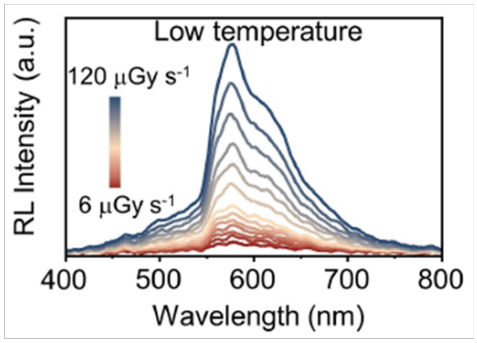
Low temperature
120 μGy s-1
6 μGy s-1
RL Intensity (a.u.)
Wavelength (nm)

F

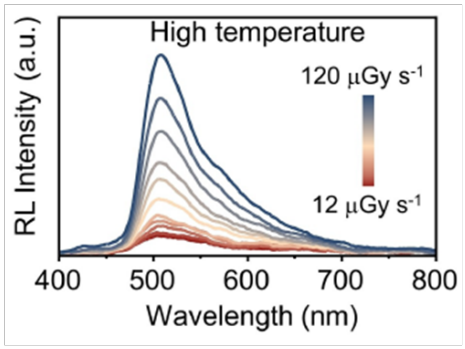
High temperature
120 μGy s-1
12 μGy s-1
RL Intensity (a.u.)
Wavelength (nm)

G

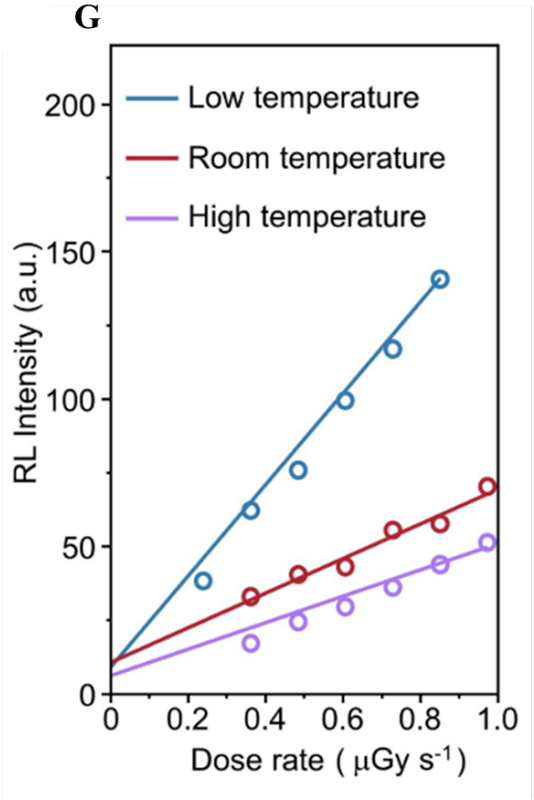
Low temperature
Room temperature
High temperature
RL Intensity (a.u.)
Dose rate (μGy s-1)

Figure 3C. Charge transfer in TADF molecules and their X-ray scintillation properties (A) Absorbance and emission spectra of $CsPbBr_3$ and difluoroboron 1,3-diphenylamine β-diketonate. (B) Schematic diagram of the charge transfer from perovskite nanosheets to TADF molecules.[18] Copyright 2022 American Chemical Society. (C) Formation of the rigid organic–inorganic hybrid perovskite $TpyBiCl_5$, which demonstrates TADF properties. (D-F) RL spectra at room, low, and high temperatures under different dosages. (G) Copyright 2024 Wiley-VCH.[57]

rate, especially at specific temperatures. The detection limit also improves from 73.04 $nGys^{-1}$ at room temperature to 38.92 $nGys^{-1}$ at 213 K and remains stable at 196.31 $nGys^{-1}$ at 353 K. These findings highlight the potential of multi-state emitting hybrid perovskites in mitigating thermal quenching in scintillators.

The obstacles posed by lead toxicity and air stability present significant challenges in advancing the development of X-ray scintillators and expanding the applications of halide perovskites. Despite sincere efforts to explore lead-free alternatives like 3D $Cs_2AgBiBr_6$ and $A_3Bi_2X_9$ (where A can be Cs^+, Rb^+, MA^+, and X includes $Cl^–$, $Br^–$, and $I^–$), devices based on these materials still fall short of the performance seen in lead-based counterparts. Overcoming this performance disparity requires a comprehensive approach, involving the optimization of growth methods, the exploration of innovative device designs, and the pursuit of advanced lead-free perovskite materials.

Effectively addressing environmental concerns linked to MHPs necessitates the adoption of robust encapsulation strategies. Currently, MHP-based X-ray detection is in its early stages, with scintillators limited to laboratory-scale production. However, future progress is anticipated, with a dedicated focus on achieving reproducibility, scaling up processing capabilities, and ensuring environmental compatibility. These advancements are crucial for

achieving the ultimate goal of commercialization. The collaborative endeavors of researchers, scientists, and engineers will be pivotal in overcoming these challenges and driving the field toward practical, large-scale applications across various industries.

3.2 Excited state engineering

The limited scintillation light yield of non-TADF organic scintillators is primarily due to the restricted contribution of triplet excited states to the scintillation process. For instance, in the case of a commercially available p-xylene-based liquid scintillator, EJ-309, the scintillation light yield is measured at 12,000 photons per MeV. Notably, p-xylene exhibits singlet and triplet excited states with energies of 2.05/100 eV and 2.35/100 eV, respectively. Given that scintillation is predominantly derived from singlet excited states, approximately half of the singlet excited states contribute to the scintillation, while the contribution from the triplet excited states remains relatively low.[58] In TADF materials, the small energy separation between the triplet and singlet excited states allows for the efficient harvesting of triplet excitons through an RISC process. This leads to delayed fluorescence from the singlet excited state, resulting in a high PLQY. Excited-state species (e.g., electronically excited atoms or molecules) and radical species that have unpaired electrons fundamentally differ in their nature under ionizing radiation compared with low-energy photoexcitation. In the latter case, organic molecules are typically excited to a singlet excited state, which can undergo high-efficiency radiative decay to the ground state, resulting in strong luminescence. In contrast, high-energy radiation, such as gamma rays or X-rays, can ionize molecules, creating secondary electrons and ions. When this ionization process occurs, a significant fraction of the excited states generated in the material are in the form of triplet states in which the spins of the electrons involved are parallel. Triplet states have longer lifetimes compared to singlet states, where the electron spins are antiparallel. As a result, the triplet states can undergo various relaxation

processes, leading to scintillation losses. Recently, several TADF molecules have been used X-ray scintillation and X-ray imaging. We present the structure of selected TADF molecules in **Scheme 4** and summarize the scintillation properties of TADF molecules in **Table 1,** including pure organic, all-inorganic, and hybrid organic–inorganic molecules. All of these materials offer an excellent light yield, reaching as high as 73,500 with a spatial resolution as low as 3.7 lp/mm. However, it is important to establish selection rules for the use of TADF materials in X-ray scintillator applications. First, TADF materials must have energy levels that closely align with the energy of X-ray photons, ensuring efficient absorption and subsequent emission. This alignment relies on appropriately positioning the highest occupied molecular orbital (HOMO) and lowest unoccupied molecular orbital (LUMO) levels relative to the X-ray energy range of interest. Second, efficient triplet harvesting is required. TADF materials need to efficiently convert triplet excitons generated by X-ray absorption into emissive singlet states. Achieving this balance between ISC and RISC rates typically involves incorporating donor–acceptor moieties with small singlet–triplet energy gaps. Third, high PLQYs are crucial for TADF materials intended for use in X-ray scintillators. Maximizing the PLQY enhances the emission intensity and improves the detection sensitivity, thus the molecular structure and solid-state morphology need to be optimized to minimize non-radiative decay pathways and enhance radiative recombination. Long-term stability is another key consideration; TADF materials should demonstrate stability under X-ray irradiation and practical operating conditions to ensure reliable performance over extended periods. This requires the design of chemically robust molecular structures or the inclusion of stabilizing additives or ligands. Fourth, processability and compatibility are essential factors to consider. TADF materials should be compatible with common fabrication processes and substrate materials used in X-ray scintillator devices, including solution processing, film formation, and flexible or rigid substrates. Finally, tunable emission properties are advantageous for tailoring TADF materials

to specific X-ray imaging applications. Customization of the emission wavelength, bandwidth, and decay kinetics enables the development of scintillator materials suitable for various imaging modalities such as radiography, fluoroscopy, and computed tomography (CT). By adhering to these selection rules, researchers can identify and design TADF materials optimized for X-ray scintillator applications, ultimately leading to the development of high-performance detectors with improved sensitivity, resolution, and reliability for a wide range of imaging tasks.

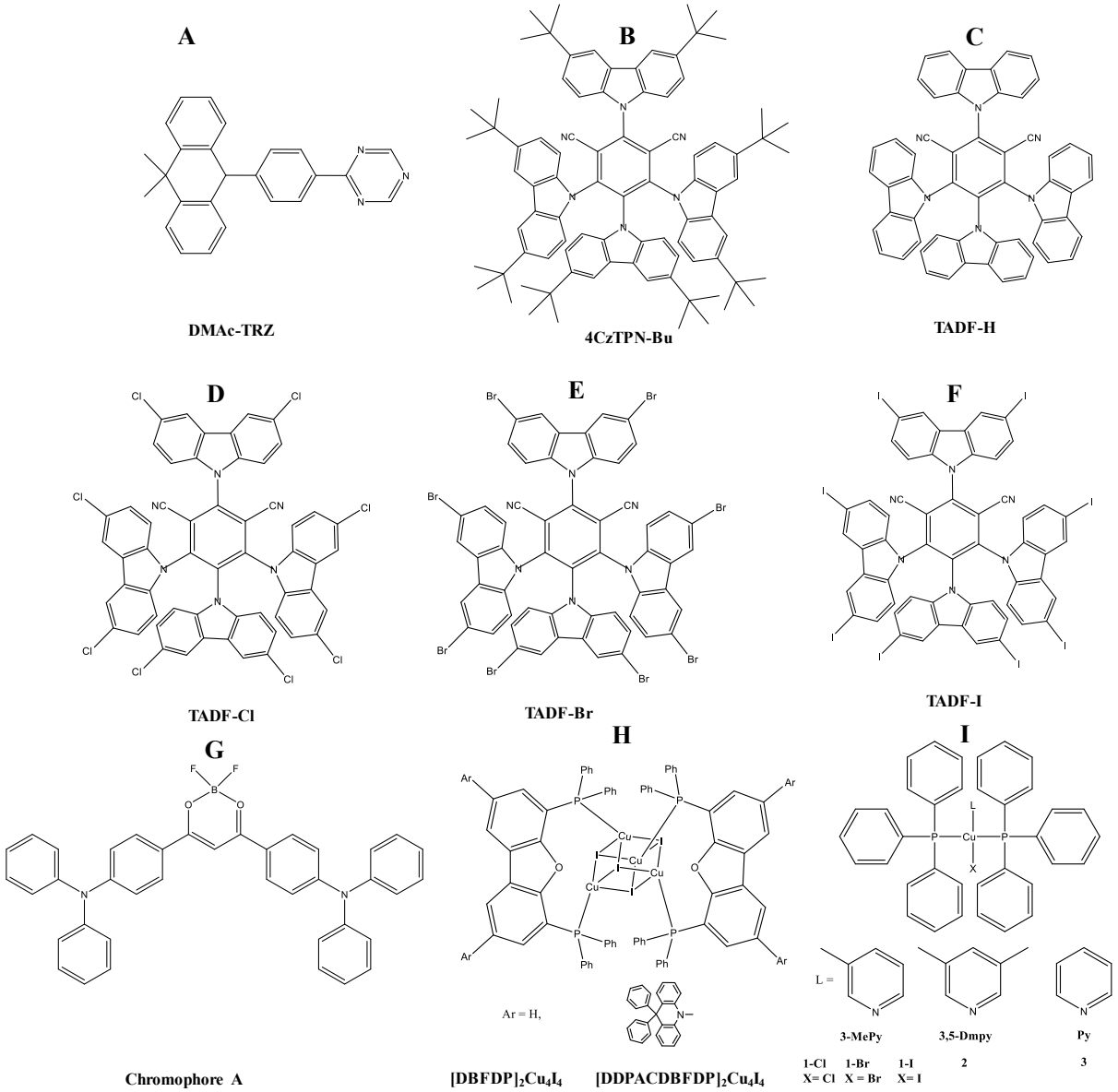

Scheme 4. Various organic and organic–inorganic TADF molecules used in X-ray scintillation and X-ray imaging.[14,18,59–61](A-G) Organic TADF molecules. (H-I) Organic-inorganic hybrid TADF molecules.

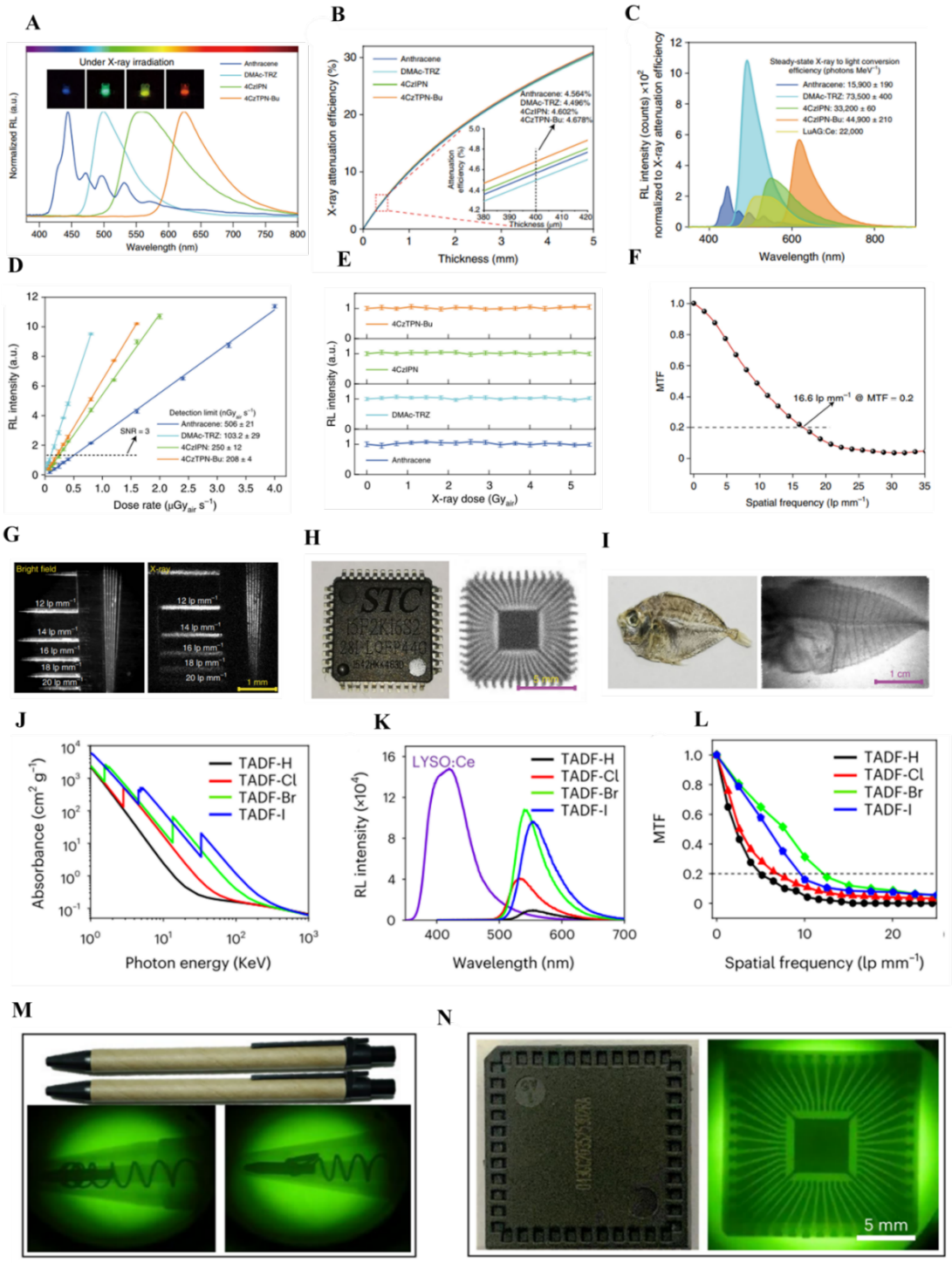

Figure 4. (A) Normalized radioluminescence (RL) spectra for anthracene, DMAc-TRZ, 4CzIPN, and 4CzTPN-Bu. (B) Calculated X-ray attenuation efficiency. (C) RL intensity spectra and light yield. (D) Detection limit. I Normalized RL intensity as a function of the dose rate. (F) MTF of the X-ray images.[14] Copyright 2022 Nature Publishing Group. (G) Bright-field (left) and X-ray (right) images of the reference plate. (H and I) Bright-field (left) and X-ray (right) images of (H) a chip and (I) a fish. RL and X-ray imaging using TADF-H, TADF-Cl, TADF-Br, and TADF-I: (J) X-ray absorption coefficient, (K) RL spectra, and (L) MTF. Bright and dark images of (M) pens and (N) an electronic chip. Copyright 2022 Nature Publishing Group.[59]

Yang et al. demonstrated three organic TADF scintillators (DMAc-TRZ, 4CzIPN, and 4CzTPN-Bu) for high-resolution X-ray imaging that captured both singlets and triplets for efficient X-ray scintillation **(Figure 4A–I)**.[14] The minimized singlet–triplet energy gap allowed these TADF chromophores to utilize both singlet and triplet excitons to emit light, resulting in higher unit exciton utilization. In comparison to anthracene, these TADF compounds displayed greater RL intensity and high X-ray attenuation efficiency. The light yields for anthracene, DMAc-TRZ, 4CzIPN, and 4CzTPN-Bu were 15,900 ± 190, 73,500 ± 400, 33,200 ± 60, and 44,900 ± 210 photons MeV^{-1}, respectively. The increased light yields observed for the TADF molecules were primarily attributed to the luminescence harvesting of triplet excitons and reduced self-absorption. The limit of detection for DMAc-TRZ was lower than the other molecules, which was in good agreement with light yields. These molecules showed little degradation under X-ray irradiation based on fatigue testing, demonstrating their suitability for practical imaging applications. A bright-field image (left) and an X-ray image (right) of a reference plate are presented in **Figure 4G**. The DMAc-TRZ:sucrose octaacetate scintillator screen produced high-quality X-ray images with line-pair notches at 16 lp mm^{-1} (**Figure 4H and I)**. Wang et al. also reported that incorporating heavy atoms (Cl, Br, and I) into TADF

chromophores can significantly enhance their X-ray absorption cross-section, which is crucial for efficient X-ray scintillation **(Figure 4J–N)**.[59] Based on X-ray absorption measurements, the researchers found a gradual increase in the resonant absorption edges and the RL intensity with the use of Cl, Br, and I. This was attributed to the heavy-atom effect, which enhances the ability of organic chromophores to absorb X-ray photons. A TADF-Br scintillation screen achieved a high resolution of 12.0 lp mm^{-1} when the MTF was 0.2. This indicates that the screen was capable of producing clear and detailed X-ray images, which was confirmed by the enhanced visualization of the spring inside a pen. Additionally, the complex structure of an electronic chip, which is typically difficult to observe, was clearly visible.[59]

The practical implementation of TADF-Br scintillation screens faces challenges related to material fabrication and stability. The synthesis and processing of these modified TADF chromophores into scintillating screens on a large scale with consistent quality particularly difficult. Ensuring the uniform distribution of heavy atoms within the material matrix is crucial for maintaining both higher X-ray absorption and TADF properties across the entire scintillation screen. Long-term stability under X-ray exposure, potential degradation mechanisms, and compatibility with different imaging environments also need careful consideration. Furthermore, achieving high-resolution X-ray imaging, as demonstrated by the 12.0 lp mm^{-1} resolution of the TADF-Br scintillation screen, may pose challenges in terms of scalability and practical applicability. The optimization of scintillator screens for specific imaging scenarios while maintaining a high resolution and sensitivity is an ongoing challenge that requires continuous refinement in material design and fabrication techniques. Overcoming these obstacles will be crucial for realizing the full potential of heavy-atom-modified TADF chromophores in efficient and reliable X-ray scintillation applications. TADF materials with a small triplet/singlet offset (ΔE_{ST}) are currently highly promising candidates for applications in scintillators. ΔE_{ST} is the energy difference between the triplet and singlet states of a molecule,

and in the context of TADF, a smaller ΔE_{ST} is desirable. The reported molecules in this category exhibit ΔE_{ST} values falling within the range of 50 to 100 meV. The ongoing interest in reducing ΔE_{ST} even further stems from the expectation that this would not only enhance the light conversion efficiency but also accelerate the RISC process.[62] However, TADF organic scintillators face certain limitations, including low X-ray absorption and a lower stopping power. To address these, a proposed solution involves combining TADF organic scintillators with high-Z materials such as heavy metal or halides which can serve as a matrix or be integrated as components. This strategic combination could resolve the low X-ray absorption and stopping power, thereby enhancing the overall performance of TADF materials in scintillation applications. The synergistic approach of leveraging the unique properties of TADF materials with the advantageous features of high-Z materials holds promise for the development of efficient and effective scintillator materials.

Metal-based TADF molecules, e.g., Cu(I) halide complexes, have also demonstrated promising results as X-ray scintillators due to their structural diversity and excellent PLQY.[60,63] Cu_4I_4 clusters have a rigid geometry that is highly beneficial for stability under X-ray irradiation and reduces relaxation-induced energy loss. Fluorescent Cu_4I_4 complexes have various charge-transfer excited states (**Figure 5)**, such as metal-to-ligand charge transfer (^{n}MLCT; n = 1 for singlet and 3 for triplet), ligand local excited states (^{n}LLE), counterion-to-ligand charge transfer (^{n}XLCT), counterion-to-metal charge transfer (^{3}XMCT), intraligand charge transfer (^{n}ILCT), and triplet cluster centered (^{3}CC) states. The excited ^{3}CC transition combines the effect of ^{3}XMCT and d→s,p metal-centered transitions, and this electronic transition reduces the radiative transition.[64] The RL mechanisms for the Cu_4I_4 cluster are similar to those for MHPs. The (M+ I)LCT process is responsible for producing the RL from Cu_4I_4 clusters. By carefully controlling the intramolecular charge transfer, the desirable (M+ I) LCT process, in which electrons are transferred from the metal center (Cu_4I_4) to the ligands,

can be promoted. This process leads to RL and can be optimized to achieve brighter and more efficient luminescence from the clusters.[60] The interplay between these different excited states and transitions necessitates careful tuning to enhance the (M+ I)LCT process responsible for RL.

Table 1: Thermally activated delayed fluorescence (TADF), metal-complex TADF, and MHP-TADF scintillators.

Ref.	Organic/Organic-inorganic hybrid materials	Photoluminescence				X-ray excited luminescence (XEL)			
		λ_{PL} (nm)	Φ (%)	τ_1, τ_2, τ_{av} (ns/μs)	Energy Gap between S_1 and T_1 (ΔE_{ST}) (cm^{-1}/meV)	λ_{XEL} (nm)	Light yield	Limit of detection (LOD)	Spatial Resolution Line pairs (lp/mm)
[14]	DMAc-TRZ	494	88.9	τ_1=20ns τ_2=2.15 μs	50-60 meV	~500	73500±400	103.2±2.9 nGy_{air} s^{-1}	16.6
	4CzIPN	501	94.4	τ_1=13.5ns τ_2= 4.76μs		~560	33200 ±60	250 ± 12 nGy_{air} s^{-1}	xx
	4CzTPN-Bu	553	80.2	τ_1=10.9ns τ_2=1.96 μs		~625	44900±210	208 ± 4 nGy_{air} s^{-1}	xx
[59]	TADF-H	~518	65	1.75	0.53 cm^{-1}	~554	1892 photons/MeV	438.5	5.1
	TADF-Cl	~521	50	1.57	0.91 cm^{-1}	~534	7076 photons/MeV	100.6	6.8
	TADF-Br	~522	48	0.72	0.94 cm^{-1}	~541	17619 photons/MeV	45.5	12.0
	TADF-I	~527	44	0.46	1.27 cm^{-1}	~552	18115 photons/MeV	45.9	9.4
[63]	$[CuCl(PPh_3)_2(3\text{-}MePy)]$	519	94.95	28.85 μs	760 cm^{-1}	525	5951 ± 135	338.8 nGy_{air} s^{-1}	xx
	$[CuBr(PPh_3)_2(3\text{-}MePy)]$	487	90.24	51.74 μs	1081 cm^{-1}	489	21 763 ± 1375	143.9 nGy_{air} s^{-1}	6.8 lp/mm

	[$CuI(PPh_3)_2$(3-MePy)]	466	93.21	63.23 µs	1027 cm^{-1}	463	28 385 ± 1335	43.8 $nGy_{air}\ s^{-1}$	9.8 lp/mm
	[$CuI(PPh_3)_2$(3,5-DmPy)]	467	91.88	34.17 µs	869 cm^{-1}	465	23 503 ± 1230	63.1 nGy_{air}	8.3 lp/mm
	[$CuI(PPh_3)_2$(Py)]	488	96.61	92.94 µs	1087 cm^{-1}	488	23 193 ± 1270	51.4 $nGy_{air}\ s^{-1}$	8.8 lp/mm
	$[DBFDP]_2Cu_4I_4$	~450, ~550 nm							
	[DDPACDBFDP]$_2Cu_4I_4$	~525 nm	71					77 nGy S−1	12 lp/mm
[65]	Singlet fission-based scintillator [Rubrene+TADF-Br]	450-650 nm	xx	1190 ns	0.16 eV	450-650	19700	1.26 $mGys^{-1}$	27.5 lp/mm
[66]	Cs_2ZrCl_6 @PDMS	447 nm	70	15.56 µs	0.069 eV	~460	49400 photons/MeV	65 $nGy_{air}\ s^{-1}$	18 lp/mm
[18]	$CsPbBr_3$ nanosheet-chromophore A	510, 620	xx	2.47 ± 0.10 ns, 61.21 ± 0.54 µs	xx	510, 620	xx	38.7 nGy/s	135 µm or 3.7 lp/mm
[67]	TADF-Br (D) and Ir-OMC (A)	530	xx	xx	xx	635	~12,000 photons/MeV	~150 nGy/s	19.8 lp/mm

Achieving optimal RL efficiency requires a fine balance when promoting the desired intramolecular charge transfer, particularly from the metal center (Cu_4I_4) to the ligands. This balance is crucial for the brightness and efficiency of luminescence from the clusters. The challenge lies in precisely manipulating these intricate electronic processes, which may require advanced synthetic techniques and a strong understanding of the structure-function

relationships within the Cu_4I_4 clusters. The stability of the Cu_4I_4 clusters under X-ray irradiation is also crucial for their practical application as scintillators. While their rigid geometry is advantageous for stability, long-term effects and potential degradation mechanisms need to be thoroughly investigated to ensure sustained performance over time. Balancing structural stability with the optimization of the luminescence properties remains a significant issue that must be addressed for the successful implementation of Cu(I) halide complexes in X-ray scintillator applications.

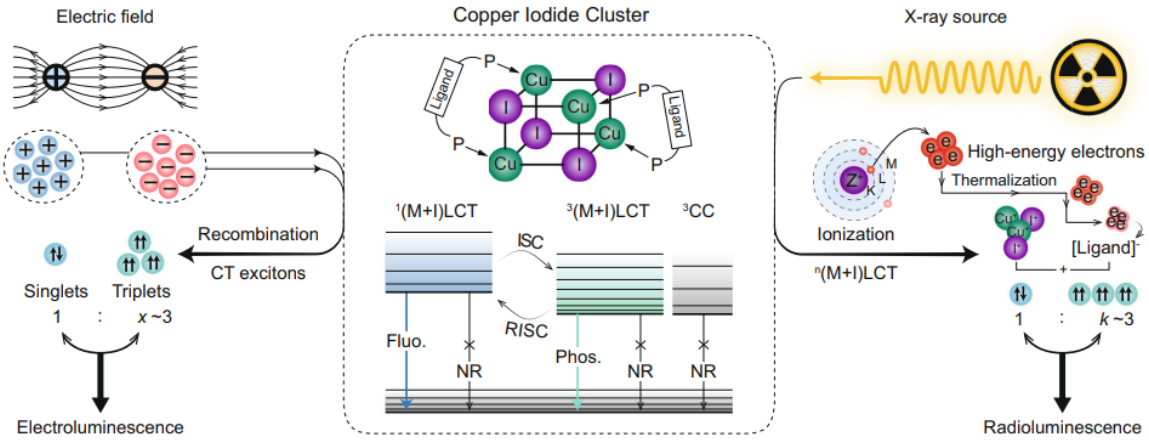

Figure 5. Charge-transfer excited states for Cu_4I_4 under X-ray radiation (center). Left: Electroluminescence mechanisms. Right: RL mechanisms.[60] Copyright 2023 Nature Publishing Group.

The development of X-ray imaging scintillators can be assisted by the investigation of novel materials that effectively transfer energy between X-ray absorber centers and luminescence chromophores. In addition to perovskite, metal–organic frameworks (MOFs) have a number of features that make them suitable for X-ray absorption in scintillator applications. First, they have outstanding X-ray absorption capabilities due to the presence of elements with a high atomic number (Z) in the metal clusters or nodes.[68] MOFs also offer remarkable structural and

compositional control, allowing for the fine-tuning of their properties. The precise selection of metal ions, ligands, and their coordination environments can optimize X-ray absorption and energy transfer processes. This flexibility enables the design of tailored MOFs with specific X-ray absorption and luminescent properties, leading to high-performance scintillators. For example, Wang et al. fabricated a Zr-based luminescent MOF-TADF (4-CzTPN-Bu) scintillator, demonstrating a nearly complete transfer of energy from the MOF to the TADF material,[67] with a very low detection limit of 256 nGy/s, far lower than that achieved by the MOF and TADF materials alone. This higher RL offers improved sensitivity and signal-to-noise ratios, making it advantageous for diagnostic and analytical purposes, such as medical imaging. However, a potential drawback is the difficulties associated with scalability and stability. Translating these findings into scalable and stable systems for practical applications may prove complex, requiring careful consideration of production processes and the stability of the charge transfer system under varying environmental conditions. These issues need to be addressed before MOF-TADF charge transfer can be reliably employed in practical, large-scale applications.

The practical use of lead-based all-inorganic perovskite materials, such as $CsPbBr_3$ NCs, as scintillators can be hampered by a number of drawbacks, such as the inclusion of the hazardous element lead, insufficient radiation stability, and substantial photon self-absorption, which reduces the efficiency of the light output. To overcome these shortcomings and advance the practical application of MHP scintillators, recent research has focused on developing alternative materials that address these challenges. Recently, Zhang et al. developed the vacancy-ordered lead-free double perovskite Cs_2ZrCl_6, which employed TADF to produce a very high PLQY of 70%.[66] Scintillator screens made from Cs_2ZrCl_6@PDMS also demonstrated excellent scintillation properties, with light yields of up to 49,400 photons/MeV of X-ray energy. Additionally, they achieved a spatial resolution of up to 18 lp mm^{-1}, thus allowing for

detailed imaging, and had a low detection limit of 65 nGy s^{-1}, indicating their ability to detect low levels of X-ray radiation. They were able to effectively capture non-planar and dynamic objects, making them suitable for various imaging scenarios. This development is expected to expand the potential application range for scintillators to different environments due to the environmental stability, high sensitivity, and low cost of the Cs_2ZrCl_6@PDMS flexible scintillator screens. However, one challenge lies in the potential long-term stability of these screens. Their environmental stability may need to be assessed over extended periods, considering factors such as temperature variation, humidity, and exposure to external elements, to ensure consistent performance over time. Additionally, the scalability of the production process may prove difficult. Transitioning from laboratory-scale fabrication to large-scale manufacturing while maintaining a uniform quality and performance characteristics is complex. Furthermore, the optimization of the Cs_2ZrCl_6@PDMS formulation for different imaging scenarios or specific applications may require further research to address potential trade-offs between flexibility, sensitivity, and imaging detail. Despite these challenges, overcoming them could lead to the broader application of Cs_2ZrCl_6@PDMS scintillator screens in diverse environments.

Flexible TADF-based X-ray scintillators are imperative due to several pressing needs in the field of medical imaging and beyond. In recent times, there has been significant interest in flexible devices due to their exceptional foldability, impressive crack resistance, excellent compatibility, and promising potential for use in portable and wearable technology. Traditional scintillator materials, such as alkali metal halides, bismuth germanate, and gadolinium oxysulfide, suffer from limitations including the need for high temperatures and vacuum conditions for fabrication, harmful scintillation decay, and unsatisfactory light yields.[42,69] These drawbacks hinder the development of low-dose, high-resolution, large-area, and flexible X-ray detectors,[70] which are essential for applications ranging from medical diagnostics to

industrial inspection. There are several reports on non-TADF organic-inorganic hybrid materials-based flexible X-ray scintillators[71] as compared to TADF materials. Xu et al. reported a flexible 0D organic manganese (II) bromide (($C_{38}H_{34}P_2$)$MnBr_4$) [$C_{38}H_{34}P$= ethylenebis-triphenylphosphonium] X-ray scintillator with a detection limit of 461.1 nGy s^{-1}.[72] TADF materials offer a solution by combining high sensitivity with flexibility, enabling their integration into bendable, conformal, and lightweight substrates. Moreover, their low fabrication temperature and tailorable properties through molecular design make them compatible with flexible systems and allow for customization to meet specific imaging requirements. By addressing these limitations, TADF-based flexible X-ray scintillators promise to revolutionize X-ray imaging by providing a versatile and efficient detection platform capable of delivering high-quality images while minimizing radiation exposure. Liu et al. synthesized flexible and bendable Cu-based TADF X-ray scintillator using PMMA and [$CuI(PPh_3)_2$(3-methylpyridine)] (**Scheme 4I**) which was used for capturing high-resolution images with a spatial resolution of 9.8 lp/mm.[73] These offers a promising method to enhance RL by integrating heavy halogen elements into TADF materials offering potential for developing affordable, high-performance scintillators.

3.3 Surface plasmonic engineering

3.3.1 Afterglow

The deposition of Ag NPs on a thin-film Lu_2SiO_5:Ce (LSO) scintillator, which is an important scintillator for nuclear medical imaging, demonstrated more rapid luminescence decay, thus rendering it useful for achieving the timing resolution required for scintillation detection.[74] Excited emitters undergo much stronger Purcell effects due to the enhanced photonic mode density of localized SPs, consequently accelerating the spontaneous recombination rate into SP modes (rather than photons in free space). The excited SPs in turn reradiate photons into free

space, resulting in the faster decay of time-resolved luminescence. Though the metal-induced ohmic loss of SPs needs to be minimized by choosing the nanostructures with the appropriate metals and size/shape to prevent deterioration of external quantum efficiency of scintillators, the inherent properties of plasmon-induced faster luminescence improves the timing resolution of scintillators, thus mitigating their afterglow effects.

3.3.2 Light yield

SP engineering has been used to improve the light yield of UV photon-excited emitters from MHPs. SP-induced light yield enhancement arises mainly from characteristic local-field enhancement. In particular, the use of appropriate metal nanostructures can tailor plasmonic dispersion relations to select specific wavelengths and momenta for plasmonic resonance in the visible or near-infrared wavelength bands. Nanostructures containing noble metals such as Au and Ag have been widely employed to achieve the sub-diffraction confinement of fields to promote the strong coupling of plasmons with luminescent centers.

Figures 6A-C present a hybrid perovskite structure and the corresponding lasing characteristics obtained from a low-temperature (77 K) PL experiment.[75] A lead halide perovskite $CH_3NH_3PbI_3$ ($MAPbI_3$) was capped with a nanometer-thick Ag film with a spacer layer of polymethylmethacrylate (PMMA; **Figure 6A)**. Across the nanometer-thick spacer layer, the UV-excited excitons in the $MAPbI_3$ were involved in near-field interactions with the Ag film whose roughness was induced by the perovskite surface morphology leading to the excitation of localized SPs. This extended the local field to the perovskite film region. Exciton-plasmon coupling led to a reduction in the lasing threshold pump power while the considerable spectral narrowing of the PL and a dramatic increase in its peak intensity occurred above the threshold. This clearly illustrates the improvement that is possible in the lasing characteristics when using plasmon-perovskite hybrid materials.

The coupling of the localized SPs of Au nanorods with $MAPbI_3$ embedded in PMMA was also demonstrated to reduce the threshold pump power for amplified spontaneous emission (ASE; **Figure 6D)**.[76] As the excitation energy increased beyond the threshold, the ASE spectrum became much narrower, while its peak was considerably higher (**Figure 6E**). It was revealed that the use of Au nanorods, whose LSPR overlapped significantly with the PL spectra, enhanced the ASE intensity at a reduced threshold energy (**Figure 6F)**. It was also found that a PMMA spacer needed to be inserted between the Au nanorods and the perovskite to avoid the metal-induced quenching of perovskite emitters.

It has also been demonstrated that SPs could enhance the coupling strength between cavity photons and perovskite excitons to produce a strong coupling regime in which the Rabi splitting energy was greater than the dissipative energy.[77] A micrometer-long nanowire of the Pb halide perovskite $CH_3NH_3PbBr_3$ ($MAPbBr_3$) was fabricated with both end facets reflective, forming a microcavity. These nanowire-based microcavities were made on an Ag nano-film with a SiO_2 spacer layer inserted between them (**Figure 6G)**. The plasmonic modes were excited due to their much smaller effective volume (lower panel) than the photonic mode volume found in the glass substrate (upper panel). The Ag-film-supported SPs increased the photonic mode density in the microcavity, increasing the Rabi splitting of exciton anti-crossing compared to the case with no Ag nano-film (**Figure 6H)**. This was due to the stronger exciton–photon coupling driven by plasmon local-field enhancement. **Figure 6I** presents the time-resolved PL of a plasmon–perovskite nanowire microcavity. When the Ag film thickness was optimized at 5 nm for SP-induced local field enhancement, the decay time constant decreased due to the non-radiative energy transfer from excitons to SPs.

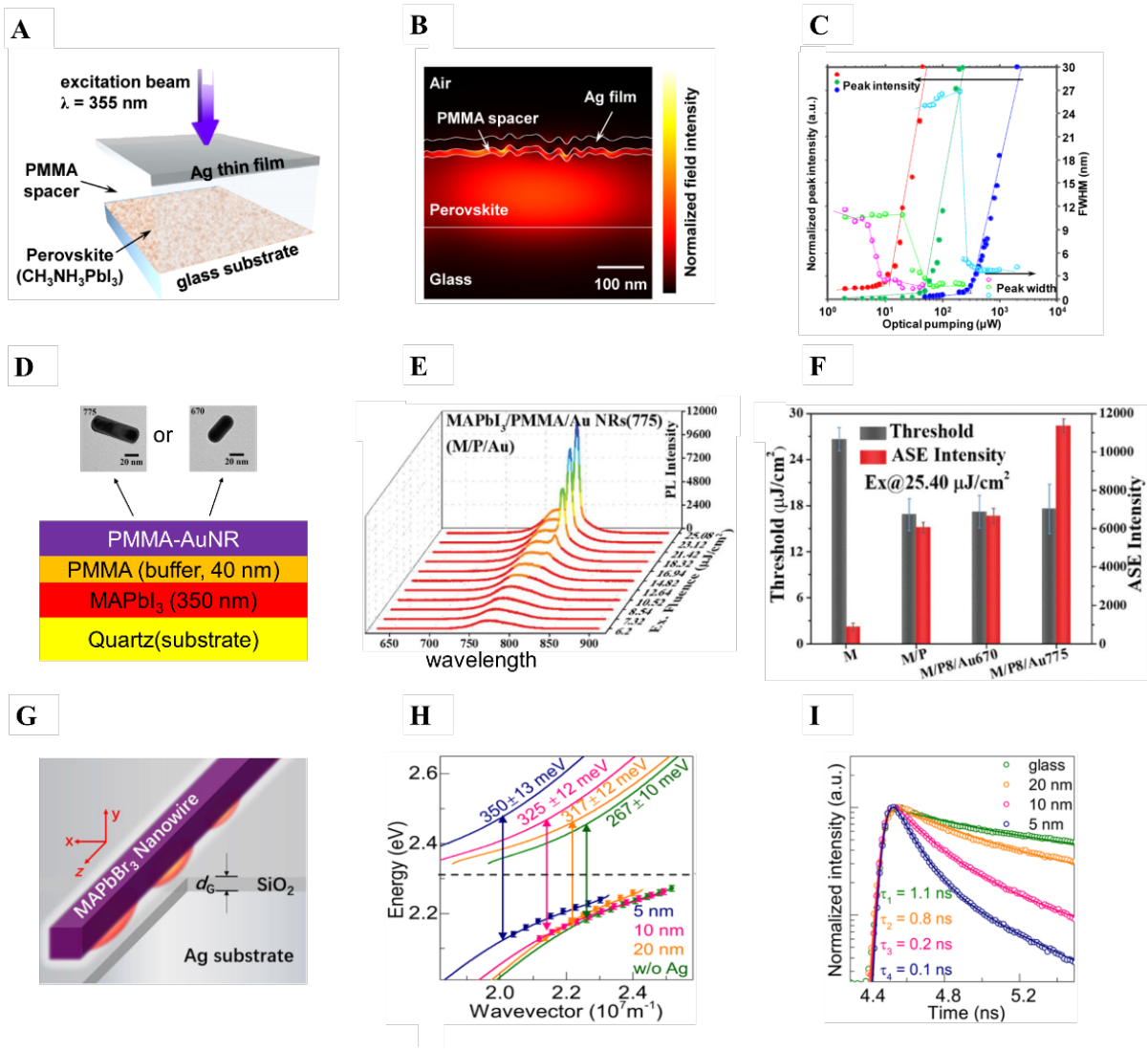

Figure 6. SP-induced improvement of MHP optoelectronic properties. (A) A schematic structure of $MAPbI_3$/PMMA/Ag thin film. (B) Field strength distribution across the layers. (C) Threshold pump power (355 nm) for 753-nm lasing from three different layers, i.e., a bare perovskite film, a perovskite film/Ag thin film, and a perovskite film/20-nm PMMA layer/Ag thin film. Reproduced with permission.[75] Copyright 2016, The Optical Society of America. (D) Schematic of the PMMA buffer layer in an Au nanorod/$MAPbI_3$/substrate structure and TEM images of Au nanorods (SPR at 670 and 775 nm). (E) Pump energy-dependent ASE spectra for $MAPbI_3$/8 nm PMMA/Au nanorods (SPR at 775 nm). (F) Comparison of ASE properties using LSPR at 670 nm. Enhancement of the ASE intensity of $MAPbI_3$ using Au nanorods whose LSPR overlaps with the PL spectra. Reproduced with permission.[76] Copyright

2019, The Royal Society of Chemistry. (G) Schematic of $MAPbBr_3$ nanowires on SiO_2 as a spacer layer and an Ag substrate and (H) cross-sectional profiles of photonic modes on a glass substrate (upper) and on a SiO_2/Ag substrate (upper). (I) Time-resolved PL spectra for $MAPbBr_3$ nanowires. Reproduced with permission.[77] Copyright 2018, American Chemical Society.

Metallic thin films have also been used to promote the plasmonic enhancement of luminescence from $CsPbBr_3$ perovskite QDs.[78] In particular, nanometer-thick Ag films increased the radiative rate and quantum efficiency within emission channels due to SPs–QDs coupling, with the 60 nm-thick Ag film producing the maximum PL intensity (**Figure 7A)**. **Figure 7B** presents the dependence of the PL intensity on the dielectric spacer layer thickness, with the 10 nm thickness generating the maximum PL intensity. This indicated that the QDs were quenched when they were in close contact (< 10 nm) while plasmon-induced local field enhancement was weaker when the QD–Ag film spacing increased to above 10 nm. The PL enhancement was highest (an ~11-fold increase) when 60 nm QDs were used with a 10-nm-thick spacer layer (**Figures 7C and D)**. This technique could be useful for improving the luminescence of materials with a low quantum efficiency.

Plasmonic enhancement for light-emitting diodes (LEDs) using perovskite materials as the gain media has also been demonstrated, with a higher internal quantum efficiency and energy extraction efficiency. Noble metal nanostructures (which could also be used as electrodes) were used for this enhancement in the LEDs, with perovskite materials such as $MAPbI_3$,[79,80] $MAPbI_{3-x}Cl_x$[81], $MAPbBr_3$,[82,83] and $CsPbBr_3$,[84–86] employed to generate the excitons.

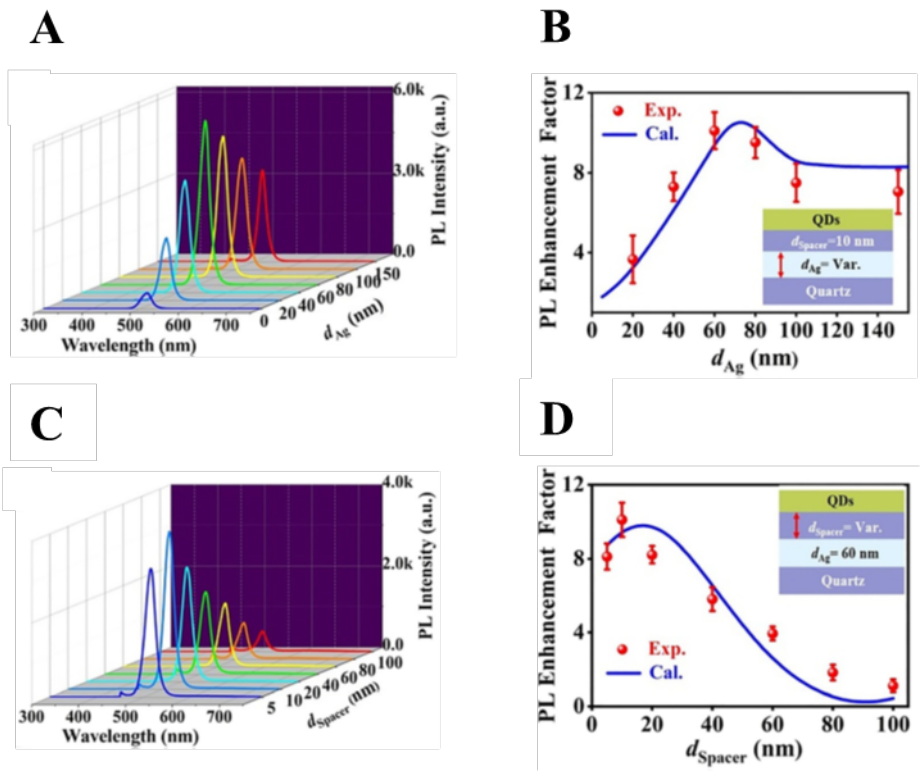

Figure 7. (A) PL spectra of $CsPbBr_3$ QDs placed on Ag films of varying thickness (d_{Ag}=0, 20, 40, 60, 80, 100, and 150 nm) with a 10-nm-thick SiO_2 spacer layer. (B) PL enhancement factor versus d_{Ag}. (C) PL spectra for $CsPbBr_3$ QDs placed on a 60-nm thick Ag film with a SiO_2 spacer layer of varying thickness (d_{spacer}=5–100 nm). (D) PL enhancement factor versus d_{spacer}. Reproduced with permission.[78] Copyright 2021, De Gruyter Academic Publishing

The LED structure was rationally designed with an appropriate distance between the perovskite and metal nanostructure by inserting a dielectric spacer with an optimized thickness to promote near-field coupling and thus excite the plasmons. The excitonic coupling rate for the plasmons was larger than that for conventional radiative recombination.[87] Various plasmonic structures have been demonstrated to transform excited plasmonic energy into luminescence, including metal grating and metal NPs. These structures compensate for the light momentum mismatch between the air and SPs when converting plasmonic energy to luminescence, thus enhancing the energy extraction efficiency. The efficient outcoupling of

plasmon energy into luminescence ultimately enhanced the net internal quantum efficiency of the LEDs.

Applying a similar approach, we propose that integrating metal nanostructures such as metal gratings or NPs into scintillator design could facilitate near-field coupling, thus enhancing the conversion of X-ray energy into luminescence. These plasmonic structures help to compensate for the momentum mismatch between X-ray-induced surface plasmons (SPs) and the scintillation process, facilitating the extraction of energy from the SPs and enhancing the overall luminescence efficiency of the scintillator.[22] This approach ultimately increases the net internal quantum efficiency of the X-ray scintillator, improving its sensitivity and performance in detecting X-ray radiation.

4. CONCLUSION AND OUTLOOK

4.1 Metal halide perovskites and thermally activated delayed fluorescence chromophores

MHP materials have been extensively studied in recent years due to their excellent optoelectronic properties, such as high quantum yields and high absorption coefficients, which make them highly attractive for various optoelectronic applications, including X-ray scintillation and imaging.[1,19,88] When incorporated into TADF scintillators, MHPs can improve the X-ray-to-visible photon conversion efficiency and thus the sensitivity of the scintillators.[18] The large cross-section of X-ray absorption in MHPs due to the presence of heavy atoms with a high Z enables the efficient conversion of X-ray photons into the excitation of TADF luminescent centers, laying the foundation for high signal-to-noise ratios and good imaging performance. However, heavy atoms have an adverse effect on the luminescence in the absence of TADF materials because they cause the non-radiative decay of singlet excited states, leading to fluorescence quenching. Unlike conventional fluorescent materials, TADF materials benefit from the energy harvesting of triplet excited states for luminescence by converting them to

singlet states via thermal energy, otherwise they would decay non-radiatively into heat. These processes result in faster luminescence decay (i.e., on a nanosecond or sub-microsecond scale) than conventional X-ray scintillators (milliseconds), allowing for X-ray detection with reduced afterglow without compromising the light yield.

It should also be noted that halogenation effects on the RL properties (from X-ray absorption to visible photon emission) of halogenated TADF materials need to be investigated in more detail. This is because the introduction of halogen atoms to TADF materials may affect the overall electronic structure and energy levels, influencing RL efficiency. Nevertheless, we can conclude that the combination of TADF materials with MHP scintillators can lead to improved temporal resolution and higher light yields, leading to improved image quality and high-speed X-ray imaging, which is particularly important for medical and industrial imaging.

4.2 Halide perovskite–plasmonic materials

MHP-based scintillators can emit fluorescence at visible wavelengths when exposed to X-rays. MHP materials absorb X-ray photons very efficiently due to the presence of high-Z atomic elements such as Pb and Cs. Excitons can be generated through multiple cascading ionization and scattering processes involving energetic carriers. Consequently, fluorescence results from the radiative recombination of electron–hole pairs, which is then detected by visible-light image sensors. However, this process faces two challenges when attempting to harness it for use in highly sensitive X-ray imaging: first, the light yield needs to be enhanced when converting X-ray-generated excitons to luminescence. Second, luminescent light has to be extracted into air with high efficiency.

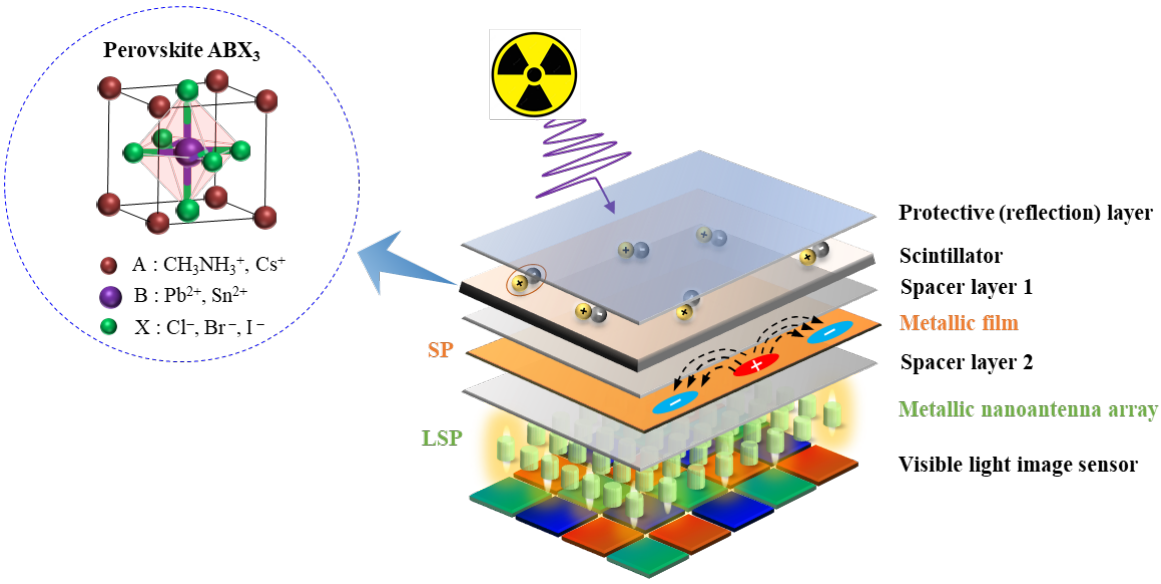

Figure 8. Schematic of the proposed structure of an MHP-based X-ray scintillator using SP technology to enhance the light yield and luminescence extraction efficiency.

In this context, plasmonic technologies can be employed to satisfy both requirements. As shown in **Figure 8**, incident X-rays that travel through the protective layer excite excitons in the perovskite material. The excited excitons can then make a near-field coupling with the noble metallic film (i.e., the plasmonic layer), with tens of nanometer thickness, generating SPs.[89–93] This coupling can be optimized through a spacer layer (spacer layer 1 in Figure 7), e.g., a dielectric film with a thickness of $\leq$50 nm[89–93], which prevents the metal-induced quenching of excitons. As a result, the generated SPs at the metal–dielectric interface enables another channel to be created for excited excitons to decay, shortening their lifetime. This also suppresses the other non-radiative decay rate of excitons whereas energy of the generated SPs can be converted into far-field luminescence when the luminescent light is appropriately extracted into air. Therefore, the use of exciton–SP coupling results in a higher internal quantum efficiency and faster decay of luminescence, both of which are favorable for

producing high temporal resolutions and a high image contrast (highly sensitive) in X-ray imaging.

Additional metallic nanostructure consisting of an array of nanoantennas with another spacer layer (spacer layer 2) can be inserted between the metallic film and visible light image sensors to extract SP energy into far-field luminescence using plasmon–plasmon coupling (i.e., delocalized SPs–localized SPs) as shown in **Figure 8**.[89–91] Without this plasmonic nanoantenna array, one might use a transparent dielectric layer below the metallic film to outcouple SPs-coupled luminescence into it. The luminescent light would then be trapped inside the transparent layer with its refractive index typically larger than air, due to total internal reflection, and consequently a small portion of light reaches the image sensor. Therefore, nanoantenna structure is required to improve the external quantum efficiency of the RL for X-ray imaging.

In general, enhancing the light extraction efficiency is vital for optical devices such as light emitting diodes, laser diodes, and display devices. In the scintillator device that we discussed, high refractive index material interfaced with air would confine light energies due to total internal reflection, making it difficult to achieve the high sensitivity of sensing visible luminescent light upon X-ray illumination. A photonic band-gap structure that imposes the index periodicity of a dielectric medium of high refractive index, can also be utilized to enhance the extraction efficiency. However, the proposed structure in this perspective uses surface plasmonic engineering which enhances not only the extraction efficiency but also the internal quantum efficiency of luminescence. One might think that a photonic bandgap structure can be shaped in the spacer layer 2 in **Figure 7**, to harvest both benefits, i.e., enhancing the internal quantum efficiency of luminescence (by metallic film-plasmon coupling with luminescent centers), and extraction efficiency (by the photonic bandgap structure). However, given the evanescent field penetration depth (at most 200 nm at visible wavelengths) of metallic film

surface plasmons (<200 nm at visible wavelengths), the photonic bandgap structure needs to be engraved within such a shallow depth in the dielectric layer, which remains a practical challenge in terms of fabrication. Therefore, a metallic nanoantenna array for outcoupling light into air (i.e., towards the display sensor) was chosen as the proposed structure for efficient light extraction in this perspective.

Overall, the proposed hybrid structure containing plasmonic technology combined with MHPs has the potential to improve the internal quantum yield, temporal resolution, and luminescence extraction efficiency, leading to high-speed X-ray scintillators with enhanced sensitivity and greater image quality. This proposed hybrid scintillator can also reduce the X-ray dose required for imaging, ultimately decreasing the patient's radiation exposure without compromising the image quality or resolution.

4.3 Designing multi-layered hybrid scintillators

Multi-layered scintillators can combine the unique advantages of different materials, including optical waveguide materials, e.g., anodized aluminum oxide templates[93] and silicon arrays,[94] and TADF materials, to optimize scintillator performance for specific X-ray imaging applications. By confining light within pores or waveguides with a high refractive index, the scintillation photons are directed toward the detector, resulting in improved light collection efficiency. This, in turn, leads to a higher spatial resolution and signal-to-noise ratio for scintillation and X-ray imaging applications. For example, a multi-layered scintillator could consist of a thin silicon array scintillator screen on top of a TADF layer. The silicon array could reduce the scattering of light and enhance the excitation rate of the perovskite scintillator by concentrating the excitation energy into smaller volumes, while the TADF layer could improve the temporal resolution by reducing the scintillation decay time. By optimizing the layer thickness and material composition, a multi-layered scintillator can be tailored to meet the

specific requirements of various X-ray imaging applications, such as medical or industrial imaging. Additionally, the use of multi-layered scintillators can also help to minimize the limitations of individual materials and improve overall scintillator performance, resulting in better image quality and higher sensitivity. In summary, the design of multi-layered scintillators is a promising approach for the optimization of the performance of X-ray scintillation and imaging systems, and there remains great potential for future research and development in this field.

Acknowledgments

This work was supported by the National Research Foundation of Korea (NRF) grant funded by the Korea government (nos. 2021R1F1A1062528, 2021R1A4A5031805, RS-2023-00236798, 2022R1F1A070724, and RS-2023-00279149)

Conflict of Interest

The authors declare no conflict of interest.

Keywords

Thermally activated delayed fluorophore; plasmonic; halide perovskites; X-ray scintillators; light yield.

REFERENCES

1. Jana, A., Cho, S., Patil, S.A., Meena, A., Jo, Y., Sree, V.G., Park, Y., Kim, H., Im, H., and Taylor, R.A. (2022). Perovskite: Scintillators, direct detectors, and X-ray imagers. Mater. Today *55*, 110–136. 10.1016/j.mattod.2022.04.009.
2. Li, Z., Zhou, F., Yao, H., Ci, Z., Yang, Z., and Jin, Z. (2021). Halide perovskites for high-performance X-ray detector. Mater. Today *48*, 155–175.

10.1016/j.mattod.2021.01.028.

3. Wu, H., Ge, Y., Niu, G., and Tang, J. (2021). Metal Halide Perovskites for X-Ray Detection and Imaging. Matter *4*, 144–163. 10.1016/j.matt.2020.11.015.

4. Zhou, Y., Chen, J., Bakr, O.M., and Mohammed, O.F. (2021). Metal Halide Perovskites for X-ray Imaging Scintillators and Detectors. ACS Energy Lett. *6*, 739–768. 10.1021/acsenergylett.0c02430.

5. Zhou, F., Li, Z., Lan, W., Wang, Q., Ding, L., and Jin, Z. (2020). Halide Perovskite, a Potential Scintillator for X-Ray Detection. Small Methods *4*, 2000506. 10.1002/smtd.202000506.

6. Moseley, O.D.I., Doherty, T.A.S., Parmee, R., Anaya, M., and Stranks, S.D. (2021). Halide perovskites scintillators: unique promise and current limitations. J. Mater. Chem. C *9*, 11588–11604. 10.1039/D1TC01595H.

7. Ou, X., Chen, X., Xu, X., Xie, L., Chen, X., Hong, Z., Bai, H., Liu, X., Chen, Q., Li, L., et al. (2021). Recent Development in X-Ray Imaging Technology: Future and Challenges. Research *2021*. 10.34133/2021/9892152.

8. Cho, S., Kim, S., Kim, J., Jo, Y., Ryu, I., Hong, S., Lee, J.-J., Cha, S., Nam, E.B., Lee, S.U., et al. (2020). Hybridisation of perovskite nanocrystals with organic molecules for highly efficient liquid scintillators. Light Sci. Appl. *9*, 156. 10.1038/s41377-020-00391-8.

9. Mittal, M., Jana, A., Sarkar, S., Mahadevan, P., and Sapra, S. (2016). Size of the Organic Cation Tunes the Band Gap of Colloidal Organolead Bromide Perovskite Nanocrystals. J. Phys. Chem. Lett. *7*, 3270–3277. 10.1021/acs.jpclett.6b01406.

10. Nikl, M., and Yoshikawa, A. (2015). Recent R&D Trends in Inorganic Single-Crystal Scintillator Materials for Radiation Detection. Adv. Opt. Mater. *3*, 463–481. 10.1002/adom.201400571.

11. Vaněček, V., Děcká, K., Mihóková, E., Čuba, V., Král, R., and Nikl, M. (2022). Advanced Halide Scintillators: From the Bulk to Nano. Adv. Photonics Res. *3*, 2200011. 10.1002/adpr.202200011.

12. Singh, A.N., Kajal, S., Kim, J., Jana, A., Kim, J.Y., and Kim, K.S. (2020). Interface

Engineering Driven Stabilization of Halide Perovskites against Moisture, Heat, and Light for Optoelectronic Applications. Adv. Energy Mater. *10(30)*, 2000768. 10.1002/aenm.202000768.

13. Alomar, S.A., Wang, J.-X., Gutiérrez-Arzaluz, L., Thomas, S., Alshareef, H.N., Bakr, O.M., Eddaoudi, M., and Mohammed, O.F. (2023). TADF-Based X-ray Screens with Simultaneously Efficient Singlet and Triplet Energy Transfer for High Spatial Imaging Resolution. ACS Appl. Mater. Interfaces *15*, 34263–34271. 10.1021/acsami.3c05675.

14. Ma, W., Su, Y., Zhang, Q., Deng, C., Pasquali, L., Zhu, W., Tian, Y., Ran, P., Chen, Z., Yang, G., et al. (2022). Thermally activated delayed fluorescence (TADF) organic molecules for efficient X-ray scintillation and imaging. Nat. Mater. *21*, 210–216. 10.1038/s41563-021-01132-x.

15. Jana, A., Park, S., Cho, S., Kim, H., and Im, H. (2022). Bounce back with triplet excitons for efficient X-ray scintillation. Matter *5*, 20–22. 10.1016/j.matt.2021.12.004.

16. Qiu, W., Liu, D., Li, M., Cai, X., Chen, Z., He, Y., Liang, B., Peng, X., Qiao, Z., Chen, J., et al. (2023). Confining donor conformation distributions for efficient thermally activated delayed fluorescence with fast spin-flipping. Nat. Commun. *14*, 2564. 10.1038/s41467-023-38197-y.

17. Kundu, M.R., White, S.M., Gopalswamy, N., and Lim, J. (1994). Millimeter, Microwave, Hard X-Ray, and Soft X-Ray Observations of Energetic Electron Populations in Solar Flares. Astrophys. J. Suppl. Ser. *90*, 599–610. 10.1017/S0252921100077873.

18. Wang, J.-X., Wang, X., Yin, J., Gutiérrez-Arzaluz, L., He, T., Chen, C., Han, Y., Zhang, Y., Bakr, O.M., Eddaoudi, M., et al. (2022). Perovskite-Nanosheet Sensitizer for Highly Efficient Organic X-ray Imaging Scintillator. ACS Energy Lett. *7*, 10–16. 10.1021/acsenergylett.1c02173.

19. Wang, Y., Li, M., Chai, Z., Wang, Y., and Wang, S. (2023). Perovskite Scintillators for Improved X-ray Detection and Imaging. Angew. Chemie Int. Ed. *62*. 10.1002/anie.202304638.

20. Koch, A., Raven, C., Spanne, P., and Snigirev, A. (1998). X-ray imaging with submicrometer resolution employing transparent luminescent screens. J. Opt. Soc. Am.

A *15*, 1940. 10.1364/JOSAA.15.001940.

21. Lecoq, P., Gektin, A., and Korzhik, M. (2006). Inorganic Scintillators for Detector Systems (Springer-Verlag) 10.1007/3-540-27768-4.

22. Jeon, G.W., Cho, S., Park, S., Kim, D.W., Jana, A., Park, D.H., Kwak, J., Im, H., and Jang, J. (2023). Plasmonically-Enhanced Radioluminescence Induced by Energy Transfer in Colloidal $CsPbBr_3$ Nanocrystals via Hybridization of Silver Nanoparticles. Adv. Opt. Mater. *2300221*, 1–7. 10.1002/adom.202300221.

23. Cerrito, L. (2017). Scintillation Process and Light Detectors. In: Radiation and Detectors. In (Springer), pp. 155–170. 10.1007/978-3-319-53181-6_9.

24. Weber, M.J. (2004). Scintillation: mechanisms and new crystals. Nucl. Instruments Methods Phys. Res. Sect. A Accel. Spectrometers, Detect. Assoc. Equip. *527*, 9–14. 10.1016/j.nima.2004.03.009.

25. Peng, Q.-C., Si, Y.-B., Wang, Z.-Y., Dai, S.-H., Chen, Q.-S., Li, K., and Zang, S.-Q. (2023). Thermally Activated Delayed Fluorescence Coinage Metal Cluster Scintillator. ACS Cent. Sci. *9*, 1419–1426. 10.1021/acscentsci.3c00563.

26. Yuan, S., Zhang, G., Chen, F., Chen, J., Zhang, Y., Di, Y., Chen, Y., Zhu, Y., Lin, M., and Chen, H. (2024). Thermally Activated Delayed Fluorescent Ag(I) Complexes for Highly Efficient Scintillation and High-Resolution X-Ray Imaging. Adv. Funct. Mater. *2400436*, 1–10. 10.1002/adfm.202400436.

27. Chen, T., Xu, Y., Ying, A., Yang, C., Lin, Q., and Gong, S. (2024). Through-Space Charge-Transfer Organogold(III) Complexes Enable High-Performance X-ray Scintillation and Imaging. Angew. Chemie Int. Ed. 10.1002/anie.202401833.

28. Bignell, L.J., Mume, E., Jackson, T.W., and Lee, G.P. (2013). Plasmonic light yield enhancement of a liquid scintillator. Appl. Phys. Lett. *102*, 7–10. 10.1063/1.4807146.

29. Conti, M., Eriksson, L., Rothfuss, H., and Melcher, C.L. (2009). Comparison of Fast Scintillators With TOF PET Potential. IEEE Trans. Nucl. Sci. *56*, 926–933. 10.1109/TNS.2008.2009446.

30. Berger, M.J.. XCOM photon cross sections database. https://www.nist.gov/pml/xcomphoton-

cross-sections-database..

31. Kakavelakis, G., Gedda, M., Panagiotopoulos, A., Kymakis, E., Anthopoulos, T.D., and Petridis, K. (2020). Metal Halide Perovskites for High-Energy Radiation Detection. Adv. Sci. *7*, 1–33. 10.1002/advs.202002098.

32. Moser, S.W., Harder, W.F., Hurlbut, C.R., and Kusner, M.R. (1993). Principles and practice of plastic scintillator design. Radiat. Phys. Chem. *41*, 31–36. 10.1016/0969-806X(93)90039-W.

33. Siciliano, E.R., Ely, J.H., Kouzes, R.T., Milbrath, B.D., Schweppe, J.E., and Stromswold, D.C. (2005). Comparison of PVT and NaI(Tl) scintillators for vehicle portal monitor applications. Nucl. Instruments Methods Phys. Res. Sect. A Accel. Spectrometers, Detect. Assoc. Equip. *550*, 647–674. 10.1016/j.nima.2005.05.056.

34. Pignalosa, P., Liu, B., Chen, H., Smith, H., and Yi, Y. (2012). Giant light extraction enhancement of medical imaging scintillation materials using biologically inspired integrated nanostructures. Opt. Lett. *37*, 2808. 10.1364/OL.37.002808.

35. Liu, B., Zhu, Z., Wu, Q., Cheng, C., Gu, M., Xu, J., Chen, H., Liu, J., Chen, L., and Ouyang, X. (2017). Plasmonic lattice resonance-enhanced light emission from plastic scintillators by periodical Ag nanoparticle arrays. Appl. Phys. Lett. *110*. 10.1063/1.4982782.

36. Knapitsch, A., Auffray, E., Fabjan, C.W., Leclercq, J.-L., Letartre, X., Mazurczyk, R., and Lecoq, P. (2012). Results of Photonic Crystal Enhanced Light Extraction on Heavy Inorganic Scintillators. IEEE Trans. Nucl. Sci. *59*, 2334–2339. 10.1109/TNS.2012.2184556.

37. Zhu, Z., Wu, S., Xue, C., Zhao, J., Wang, L., Wu, Y., Liu, B., Cheng, C., Gu, M., Chen, H., et al. (2015). Enhanced light extraction of scintillator using large-area photonic crystal structures fabricated by soft-X-ray interference lithography. Appl. Phys. Lett. *106*. 10.1063/1.4922699.

38. Zhu, Z., Liu, B., Zhang, H., Ren, W., Cheng, C., Wu, S., Gu, M., and Chen, H. (2015). Improvement of light extraction of LYSO scintillator by using a combination of self-assembly of nanospheres and atomic layer deposition. Opt. Express *23*, 7085. 10.1364/OE.23.007085.

39. Vecchi, G., Giannini, V., and Gómez Rivas, J. (2009). Surface modes in plasmonic crystals induced by diffractive coupling of nanoantennas. Phys. Rev. B *80*, 201401. 10.1103/PhysRevB.80.201401.

40. Li, Y., Lei, Y., Wang, H., and Jin, Z. (2023). Two-Dimensional Metal Halides for X-Ray Detection Applications. Nano-Micro Lett. *15*, 128. 10.1007/s40820-023-01118-1.

41. Peng, G., An, B., Chen, H., Li, Z., Xu, Y., Wang, Q., Wang, T., Wang, H., Ding, L., and Jin, Z. (2023). Self-Organizing Pixelated Cs_4PbBr_6 Scintillator Plate for Large-Area, Ultra-Flexible, High Spatial Resolution and Stable X-Ray Imaging. Adv. Opt. Mater. *11*, 1–9. 10.1002/adom.202201751.

42. Mu, Y., He, Z., Wang, K., Pi, X., and Zhou, S. (2022). Recent progress and future prospects on halide perovskite nanocrystals for optoelectronics and beyond. iScience *25*, 105371. 10.1016/j.isci.2022.105371.

43. Lu, L., Sun, M., Wu, T., Lu, Q., Chen, B., and Huang, B. (2022). All-inorganic perovskite nanocrystals: next-generation scintillation materials for high-resolution X-ray imaging. Nanoscale Adv. *4*, 680–696. 10.1039/D1NA00815C.

44. Parveen, S., and Giri, P.K. (2022). Emerging doping strategies in two-dimensional hybrid perovskite semiconductors for cutting edge optoelectronics applications. Nanoscale Adv. *4*, 995–1025. 10.1039/D1NA00709B.

45. Datta, A., Fiala, J., and Motakef, S. (2021). 2D perovskite-based high spatial resolution X-ray detectors. Sci. Rep. *11*, 22897. 10.1038/s41598-021-02378-w.

46. Chen, Q., Wu, J., Ou, X., Huang, B., Almutlaq, J., Zhumekenov, A.A., Guan, X., Han, S., Liang, L., Yi, Z., et al. (2018). All-inorganic perovskite nanocrystal scintillators. Nature *561*, 88–93. 10.1038/s41586-018-0451-1.

47. Zhang, Y., Sun, R., Ou, X., Fu, K., Chen, Q., Ding, Y., Xu, L.-J., Liu, L., Han, Y., Malko, A. V., et al. (2019). Metal Halide Perovskite Nanosheet for X-ray High-Resolution Scintillation Imaging Screens. ACS Nano *13*, 2520–2525. 10.1021/acsnano.8b09484.

48. Cao, J., Guo, Z., Zhu, S., Fu, Y., Zhang, H., Wang, Q., and Gu, Z. (2020). Preparation of Lead-free Two-dimensional Layered $(C_8H_{17}NH_3)_2SnBr_4$ Perovskite Scintillators and

Their Application in X-ray Imaging. ACS Appl. Mater. Interfaces *6*, acsami.0c02116. 10.1021/acsami.0c02116.

49. Birowosuto, M.D., Cortecchia, D., Drozdowski, W., Brylew, K., Lachmanski, W., Bruno, A., and Soci, C. (2016). X-ray Scintillation in Lead Halide Perovskite Crystals. Sci. Rep. *6*, 37254. 10.1038/srep37254.

50. Blasse, G. (1994). Scintillator materials. Chem. Mater. *6*, 1465–1475. 10.1021/cm00045a002.

51. Xie, A., Hettiarachchi, C., Maddalena, F., Witkowski, M.E., Makowski, M., Drozdowski, W., Arramel, A., Wee, A.T.S., Springham, S.V., Vuong, P.Q., et al. (2020). Lithium-doped two-dimensional perovskite scintillator for wide-range radiation detection. Commun. Mater. *1*, 37. 10.1038/s43246-020-0038-x.

52. Kobayashi, M., Omata, K., Sugimoto, S., Tamagawa, Y., Kuroiwa, T., Asada, H., Takeuchi, H., and Kondo, S. (2008). Scintillation characteristics of CsPbCl3 single crystals. Nucl. Instrum. Methods Phys. Res. A *592*, 369–373. 10.1016/j.nima.2008.04.079.

53. Mykhaylyk, V.B., Kraus, H., Kapustianyk, V., Kim, H.J., Mercere, P., Rudko, M., Da Silva, P., Antonyak, O., and Dendebera, M. (2020). Bright and fast scintillations of an inorganic halide perovskite $CsPbBr_3$ crystal at cryogenic temperatures. Sci. Rep. *10*, 8601. 10.1038/s41598-020-65672-z.

54. García de Arquer, F.P., Talapin, D. V., Klimov, V.I., Arakawa, Y., Bayer, M., and Sargent, E.H. (2021). Semiconductor quantum dots: Technological progress and future challenges. Science. *373*. 10.1126/science.aaz8541.

55. Chen, W., Liu, Y., Yuan, Z., Xu, Z., Zhang, Z., Liu, K., Jin, Z., and Tang, X. (2017). X-ray radioluminescence effect of all-inorganic halide perovskite $CsPbBr_3$ quantum dots. J. Radioanal. Nucl. Chem. *314*, 2327–2337. 10.1007/s10967-017-5562-x.

56. Cho, S., Kim, S., Han, I., Jana, A., Kim, H., Kwak, J., and Im, H. (2024). Optimal design and characteristic analysis of $CsPbBr_3$ nanocrystals hybridized with 2,5-diphenyloxazole molecules for UV and X-ray detection. Mater. Today Chem. *35*, 101851. 10.1016/j.mtchem.2023.101851.

57. Wang, M., Zhang, Z., Lyu, J., Qiu, J., Gu, C., Zhao, H., Wang, T., Ren, Y., Yang, S.-W., Qin Xu, G., et al. (2024). Overcoming Thermal Quenching in X-ray Scintillators through Multi-Excited State Switching. Angew. Chemie Int. Ed. *202401949*. 10.1002/anie.202401949.

58. Koshimizu, M. (2023). Recent progress of organic scintillators. Jpn. J. Appl. Phys. *62*, 010503. 10.35848/1347-4065/ac94fe.

59. Wang, J.-X., Gutiérrez-Arzaluz, L., Wang, X., He, T., Zhang, Y., Eddaoudi, M., Bakr, O.M., and Mohammed, O.F. (2022). Heavy-atom engineering of thermally activated delayed fluorophores for high-performance X-ray imaging scintillators. Nat. Photonics *16*, 869–875. 10.1038/s41566-022-01092-x.

60. Zhang, N., Qu, L., Dai, S., Xie, G., Han, C., Zhang, J., Huo, R., Hu, H., Chen, Q., Huang, W., et al. (2023). Intramolecular charge transfer enables highly-efficient X-ray luminescence in cluster scintillators. Nat. Commun. *14*, 2901. 10.1038/s41467-023-38546-x.

61. Liu, X., Jiang, Y., Li, F., Xu, X., Li, R., Zhu, W., Ni, J., Ding, C., Liu, S., and Zhao, Q. (2023). Thermally Activated Delayed Fluorescent Scintillators Based on Mononuclear Copper(I) Halide Complexes for High-Resolution X-Ray Imaging. Adv. Opt. Mater. *11*. 10.1002/adom.202202169.

62. Endo, A., Sato, K., Yoshimura, K., Kai, T., Kawada, A., Miyazaki, H., and Adachi, C. (2011). Efficient up-conversion of triplet excitons into a singlet state and its application for organic light emitting diodes. Appl. Phys. Lett. *98*. 10.1063/1.3558906.

63. Liu, X., Jiang, Y., Li, F., Xu, X., Li, R., Zhu, W., Ni, J., Ding, C., Liu, S., and Zhao, Q. (2023). Thermally Activated Delayed Fluorescent Scintillators Based on Mononuclear Copper(I) Halide Complexes for High-Resolution X-Ray Imaging. Adv. Opt. Mater. *11*, 2202169. 10.1002/adom.202202169.

64. Xie, M., Han, C., Liang, Q., Zhang, J., Xie, G., and Xu, H. (2019). Highly efficient sky blue electroluminescence from ligand-activated copper iodide clusters: Overcoming the limitations of cluster light-emitting diodes. Sci. Adv. *5*, 1–9. 10.1126/sciadv.aav9857.

65. Wang, J., Yin, J., Gutiérrez-Arzaluz, L., Thomas, S., Shao, W., Alshareef, H.N.,

Eddaoudi, M., Bakr, O.M., and Mohammed, O.F. (2023). Singlet Fission-Based High-Resolution X-Ray Imaging Scintillation Screens. Adv. Sci. *2300406*, 1–5. 10.1002/advs.202300406.

66. Zhang, F., Zhou, Y., Chen, Z., Wang, M., Ma, Z., Chen, X., Jia, M., Wu, D., Xiao, J., Li, X., et al. (2022). Thermally Activated Delayed Fluorescence Zirconium-Based Perovskites for Large-Area and Ultraflexible X-ray Scintillator Screens. Adv. Mater. *34*, 2204801. 10.1002/adma.202204801.

67. Wang, J.-X., Gutiérrez-Arzaluz, L., Wang, X., Almalki, M., Yin, J., Czaban-Jóźwiak, J., Shekhah, O., Zhang, Y., Bakr, O.M., Eddaoudi, M., et al. (2022). Nearly 100% energy transfer at the interface of metal-organic frameworks for X-ray imaging scintillators. Matter *5*, 253–265. 10.1016/j.matt.2021.11.012.

68. Neufeld, M.J., Lutzke, A., Pratx, G., and Sun, C. (2021). High- Z Metal–Organic Frameworks for X-ray Radiation-Based Cancer Theranostics. Chem. – A Eur. J. *27*, 3229–3237. 10.1002/chem.202003523.

69. Wibowo, A., Sheikh, M.A.K., Diguna, L.J., Ananda, M.B., Marsudi, M.A., Arramel, A., Zeng, S., Wong, L.J., and Birowosuto, M.D. (2023). Development and challenges in perovskite scintillators for high-resolution imaging and timing applications. Commun. Mater. *4*, 21. 10.1038/s43246-023-00348-5.

70. Li, H., Liu, X., Yang, T., Ma, C., Du, Y., Xu, P., Zhang, L., Song, X., Cui, Q., Zhao, S., et al. (2024). Flexible Large-Scale Self-Driven Perovskite X-ray Detector by Precise Heterogeneous Integration. ACS Energy Lett. *9*, 64–74. 10.1021/acsenergylett.3c02152.

71. Wang, B., Yang, X., Chen, S., Lu, S., Zhao, S., Qian, Q., Cai, W., Wang, S., and Zang, Z. (2022). Flexible perovskite scintillators and detectors for X-ray detection. iScience *25*, 105593. 10.1016/j.isci.2022.105593.

72. Xu, L.-J., Lin, X., He, Q., Worku, M., and Ma, B. (2020). Highly efficient eco-friendly X-ray scintillators based on an organic manganese halide. Nat. Commun. *11*, 4329. 10.1038/s41467-020-18119-y.

73. Liu, X., Jiang, Y., Li, F., Xu, X., Li, R., Zhu, W., Ni, J., Ding, C., Liu, S., and Zhao, Q. (2023). Thermally Activated Delayed Fluorescent Scintillators Based on Mononuclear

Copper(I) Halide Complexes for High-Resolution X-Ray Imaging. Adv. Opt. Mater. *11*, 1–8. 10.1002/adom.202202169.

74. Liu, B., Zhu, Z., Zhu, J., Wu, S., Chen, H., Gu, M., Cheng, Q., Chen, H., Cheng, C., Wang, Z., et al. (2014). An approach to achieve significantly faster luminescence decay of thin-film scintillator by surface plasmons. Appl. Phys. Lett. *104*. 10.1063/1.4864634.

75. Kao, T.S., Hong, K.-B., Chou, Y.-H., Huang, J.-F., Chen, F.-C., and Lu, T.-C. (2016). Localized surface plasmon for enhanced lasing performance in solution-processed perovskites. Opt. Express *24*, 20696. 10.1364/OE.24.020696.

76. Wu, X., Jiang, X.-F., Hu, X., Zhang, D.-F., Li, S., Yao, X., Liu, W., Yip, H.-L., Tang, Z., and Xu, Q.-H. (2019). Highly stable enhanced near-infrared amplified spontaneous emission in solution-processed perovskite films by employing polymer and gold nanorods. Nanoscale *11*, 1959–1967. 10.1039/C8NR08952C.

77. Shang, Q., Zhang, S., Chen, J., Yang, P., Li, W., Zhang, Y., Xiong, Q., Liu, X., and Zhang, Q. (2017). Surface Plasmon Enhanced Strong Exciton-Photon Coupling in Hybrid Inorganic-Organic Perovskites Nanowires. Nano Lett. *18*, 3335–3343. 10.1021/acs.nanolett.7b04847.

78. Zhao, W., Wen, Z., Xu, Q., Zhou, Z., Li, S., Fang, S., Chen, T., Sun, L., Wang, X., Liu, Y., et al. (2021). Remarkable photoluminescence enhancement of $CsPbBr_3$ perovskite quantum dots assisted by metallic thin films. Nanophotonics *10*, 2257–2264. 10.1515/nanoph-2021-0064.

79. Xu, L., Qiang, Y., Xiao, K., Zhang, Y., Xie, J., Cui, C., Lin, P., Wang, P., Yu, X., Wu, F., et al. (2017). Surface plasmon enhanced luminescence from organic-inorganic hybrid perovskites. Appl. Phys. Lett. *110*. 10.1063/1.4985294.

80. Bayles, A., Carretero-Palacios, S., Calió, L., Lozano, G., Calvo, M.E., and Míguez, H. (2020). Localized surface plasmon effects on the photophysics of perovskite thin films embedding metal nanoparticles. J. Mater. Chem. C *8*, 916–921. 10.1039/C9TC05785D.

81. Cai, C., Zhai, J., Bi, G., and Wu, H. (2016). Electron energy transfer effect in Au NS/$CH_3NH_3PbI_{3-x}Cl_x$ heterostructures via localized surface plasmon resonance

coupling. Opt. Lett. *41*, 4297. 10.1364/ol.41.004297.

82. Shakouri, S.M., Bagherzadeh-Khajehmarjan, E., and Ahmadi-Kandjani, S. (2019). Spectral behavior of plasmon enhanced fluorescence in organic–inorganic perovskite quantum dot solutions. Phys. Scr. *94*, 055503. 10.1088/1402-4896/ab0571.

83. Chen, P., Xiong, Z., Wu, X., Shao, M., Meng, Y., Xiong, Z., and Gao, C. (2017). Nearly 100% Efficiency Enhancement of $CH_3NH_3PbBr_3$ Perovskite Light-Emitting Diodes by Utilizing Plasmonic Au Nanoparticles. J. Phys. Chem. Lett. *8*, 3961–3969. 10.1021/acs.jpclett.7b01562.

84. Zhang, X., Xu, B., Wang, W., Liu, S., Zheng, Y., Chen, S., Wang, K., and Sun, X.W. (2017). Plasmonic Perovskite Light-Emitting Diodes Based on the Ag–$CsPbBr_3$ System. ACS Appl. Mater. Interfaces *9*, 4926–4931. 10.1021/acsami.6b12450.

85. Zhang, Y., Sun, H., Zhang, S., Li, S., Wang, X., Zhang, X., Liu, T., and Guo, Z. (2019). Enhancing luminescence in all-inorganic perovskite surface plasmon light-emitting diode by incorporating Au-Ag alloy nanoparticle. Opt. Mater. (Amst). *89*, 563–567. 10.1016/j.optmat.2019.01.074.

86. Zhang, K., Zhou, D., Qiu, J., Long, Z., Zhu, R., Wang, Q., Lai, J., Wu, H., and Zhu, C. (2020). Silver nanoparticles enhanced luminescence and stability of $CsPbBr_3$ perovskite quantum dots in borosilicate glass. J. Am. Ceram. Soc. *103*, 2463–2470. 10.1111/jace.16966.

87. Gu, L., Wen, K., Peng, Q., Huang, W., and Wang, J. (2020). Surface-Plasmon-Enhanced Perovskite Light-Emitting Diodes. Small *16*, 2001861. 10.1002/smll.202001861.

88. Wu, H., Ge, Y., Niu, G., and Tang, J. (2021). Metal Halide Perovskites for X-Ray Detection and Imaging. Matter *4*, 144–163. 10.1016/j.matt.2020.11.015.

89. Cesario, J., Quidant, R., Badenes, G., and Enoch, S. (2005). Electromagnetic coupling between a metal nanoparticle grating and a metallic surface. Opt. Lett. *30*, 3404. 10.1364/OL.30.003404.

90. Cesario, J., Gonzalez, M.U., Cheylan, S., Barnes, W.L., Enoch, S., and Quidant, R. (2007). Coupling localized and extended plasmons to improve the light extraction

through metal films. Opt. Express *15*, 10533. 10.1364/OE.15.010533.

91. Fusella, M.A., Saramak, R., Bushati, R., Menon, V.M., Weaver, M.S., Thompson, N.J., and Brown, J.J. (2020). Plasmonic enhancement of stability and brightness in organic light-emitting devices. Nature *585*, 379–382. 10.1038/s41586-020-2684-z.

92. Li, C., Liu, Z., Shang, Q., and Zhang, Q. (2019). Surface-Plasmon-Assisted Metal Halide Perovskite Small Lasers. Adv. Opt. Mater. *7*, 1900279. 10.1002/adom.201900279.

93. Zhao, X., Jin, T., Gao, W., Niu, G., Zhu, J., Song, B., Luo, J., Pan, W., Wu, H., Zhang, M., et al. (2021). Embedding $Cs_3Cu_2I_5$ Scintillators into Anodic Aluminum Oxide Matrix for High-Resolution X-Ray Imaging. Adv. Opt. Mater. *9*, 2101194. 10.1002/adom.202101194.

94. Wang, H., Wang, J.-X., Song, X., He, T., Zhou, Y., Shekhah, O., Gutiérrez-Arzaluz, L., Bayindir, M., Eddaoudi, M., Bakr, O.M., et al. (2023). Copper Organometallic Iodide Arrays for Efficient X-ray Imaging Scintillators. ACS Cent. Sci. *9*, 668–674. 10.1021/acscentsci.2c01495.